الجمهورية الجزائرية الديمقراطية الشعبية
République algérienne démocratique et populaire
وزارة التعليم العالي والبحث العلمي
Ministère de l'enseignement supérieur et de la recherche scientifique
جامعة عين تموشنت بلحاج بوشعيب
Université –Ain Temouchent- Belhadj Bouchaib
Faculté des Sciences et de Technologie
Département de Génie mécanique

Projet de Fin d'Etudes
Pour l'obtention du diplôme de Master en : Génie des procédés
Domaine : Science et technologie
Filière : Génie des procédés
Spécialité : Génie des procédés des matériaux
Thème

Study of Hydrocarbon Adsorption from Industrial Effluents Using Mesoporous Materials

Soutenu le : 29/06/2025

Présenté Par :
1) Melle. SI ALI Rihab
2) Melle. RAHMOUN Imane

Devant le jury composé de :

Dr. REMLAOUI Ahmed	MCA	UAT.B.B (Ain Temouchent)	Président
Dr. YOUNES Kawther	MCB	UAT.B.B (Ain Temouchent)	Examinatrice
Dr. CHOUAT Nadjat	MCA	UAT.B.B (Ain Temouchent)	Encadrante

Année Universitaire 2024/2025

الجمهورية الجزائرية الديمقراطية الشعبية
People's democratic republic of Algeria
وزارة التعليم العالي والبحث العلمي
Ministry of Higher Education and Scientific Research
جامعة عين تموشنت بلحاج بوشعيب
University of Ain Temouchent – Belhadj Bouchaib
Faculty of Science and Technology
Department of Mechanical engineering

Final Year Project
In Partial Fulfillment of the Requirements for the Degree of Master in:
Process Engineering
Field: science and technology
Program: process engineering
Specialty: process and materials engineering
Thesis title

Study of hydrocarbon adsorption from industrial effluents using mesoporous materials

Defense date: 29/06/2025

Presented by:
1) Miss. SI ALI Rihab
2) Miss. RAHMOUN Imane

Jury Members:

Dr. REMLAOUI Ahmed	MCA	UAT.B.B (Ain Temouchent)	President
Dr. YOUNES Kawther	MCB	UAT.B.B (Ain Temouchent)	Examiner
Dr. CHOUAT Nadjat	MCA	UAT.B.B (Ain Temouchent)	Supervisor

Academic Year 2024/2025

Acknowledgements

First and foremost, we thank God Almighty for granting us the patience, strength, and perseverance to reach this important milestone in our academic journey.

We would like to express our deepest gratitude to **Mrs. CHOUAT Nadjat**, our supervisor, for her invaluable guidance, kindness, and constant availability throughout this work. Her scientific rigor, combined with her human understanding, has been a key factor in our progress and has helped us give the best of ourselves.

We sincerely thank the members of the jury **Ramlaoui Ahmed, Younes kawther** for the honor of evaluating this work, as well as for their constructive feedback, which will undoubtedly enrich our thinking.

Our thanks also go to all the staff at the GL3Z complex for their warm welcome, technical assistance, and logistical support throughout our internship.

We also extend our gratitude to our fellow classmates, with whom we have shared countless moments of doubt, perseverance, and joy during our studies.

Finally, we dedicate this work to our families, the unwavering pillar of our life. Your love, unconditional support, and constant encouragement have always been our greatest source of motivation. Thank you for believing in us, even when we doubted ourselves.

Dedications

I dedicate this work

to my beloved **mother**,

to the one whose love knows no bounds,

whose silent strength lit every step of my journey.

This achievement is not the fruit of my effort alone,

but the echo of your sacrifices, the reflection of your unwavering love,

and proof that I was never truly walking alone.

Mom,

through your quiet tenderness, your sleepless nights worrying for me, your faith in me even when I doubted myself…

You gave me the strength to believe, and what I celebrate today, I celebrate for you, with you, and because of you.

A special word to my dear **father**, for your quiet presence that always brought me peace,

and your steady strength that reassured my heart.

With all my love and gratitude,

Rihab

Dedications

To all those who are dear to me, to whom I owe my success:

To our Lord, Almighty **God**, “Thank you, God, for giving me life, faith, and answered prayers, and for allowing me to succeed.”

To **myself**, for all the sleepless nights, the silent battles fought alone. For every time I chose perseverance over giving up, and hope over fear. I am proud of the woman I’ve become strong, determined, and resilient. It’s finally time to be here. I deserve this moment.

To the one whose words have accompanied me since I was little, who suffered without letting us suffer, who taught me to be a strong, goal-driven woman, who always fights to reach her goals no matter the cost; the one who encouraged me to pursue my dreams even when obstacles seemed insurmountable. My guardian angel, your love and presence in my life, and the fact that you are **my mother**, will always guide me along my path.

To the one who once told me I was the apple of his eye, who saw in my smallest success his greatest pride, to the man who made me who I am today because he is **my father**, the one in whose eyes I saw pride in me, my role model of respect and a father’s love. Thanks to him, I have learned to be the daughter who never stops striving to make him happy and proud.

To my husband **Mohamed**, your love, patience, and unwavering support have been my strongest pillars throughout this journey. believed in me when I struggled to believe in myself, and celebrated each small victory as if it were your own. Thank you for your kindness, your encouragement, and for being my peace through every storm

To my sisters **Micho**, **kadra**, **Ghayma**, and **Khadidja**, your love has always been a source of strength for me. Thank you for being my support system, my source of laughter, and my safe space. In every step of this journey, your presence whether near or far has comforted me and reminded me that I am never alone. thanks.

To my brothers **Abdelrahman** and **Ammar**, thank you for being my constant source of encouragement and strength. You’ve always been there, silently cheering me on, and reminding me of my worth. I am truly grateful to have you by my side

To my uncle **Mimoun**, Thank you for your constant support and encouragement throughout my journey. Your presence in my life has been a blessing, and I am truly grateful for all the care and guidance you’ve given me.

To my friends, thank you for filling my journey with friendship, laughter, and unforgettable memories, and your support has given me strength when I needed it most.

And to everyone who has helped me in any way, whether through a kind word, a gesture, or silent support from afar thank you from the bottom of my heart.

Imane

Table of Contents

CHAPTER III. Adsorption and Adsorbent

CHAPTER IV. Experimental Procedures

CHAPTER V. Results And Discussion

List of figures

List of tables

Summary

This work focuses on the study of hydrocarbon adsorption from industrial effluents using mesoporous materials, particularly MCM-41 and its modified forms. These pollutants, which are often difficult to remove using conventional methods, pose a serious environmental threat. The study covers both the theoretical aspects of adsorption and its experimental applications, including the synthesis, characterization of materials, and adsorption tests. The results show that modified materials significantly improve hydrocarbon removal efficiency, especially at neutral pH. These findings highlight the potential of mesoporous materials in industrial wastewater treatment and open the door to further research on optimizing adsorption conditions, developing new adsorbents, and integrating these materials into large-scale industrial systems.

Keywords:

MCM-41, Mesoporous silica, Adsorption, Hydrocarbons, Surface modification, MDEA, Aluminum incorporation, CTABr, TEOS, pH effect, Contact time, Adsorbent dose, FTIR, BET, XRD, Isotherm models, Environmental treatment, Industrial effluents, Surface area, Selectivity.

Résumé

Ce travail de mémoire porte sur l'étude de l'adsorption des hydrocarbures à partir des effluents industriels en utilisant des matériaux mésoporeux, en particulier le MCM-41 et ses formes modifiées. Ces polluants, souvent difficiles à éliminer par les méthodes conventionnelles, représentent une menace environnementale sérieuse. L'étude aborde à la fois les aspects théoriques de l'adsorption et ses applications expérimentales, incluant la synthèse, la caractérisation des matériaux, ainsi que les tests d'adsorption. Les résultats montrent que les matériaux modifiés améliorent significativement l'efficacité de l'élimination des hydrocarbures, notamment à pH neutre. Ces résultats soulignent le potentiel des matériaux mésoporeux dans le traitement des eaux usées industrielles et ouvrent la voie à de nouvelles recherches sur l'optimisation des conditions d'adsorption, le développement de nouveaux adsorbants et l'intégration de ces matériaux dans des systèmes industriels à grande échelle.

ملخص

يركز هذا البحث على دراسة امتزاز الهيدروكربونات من المياه الصناعية باستخدام المواد المسامية، وخاصة مادة MCM-41 وأشكالها المعدّلة. تُعدّ هذه الملوثات من بين الأكثر صعوبة في الإزالة بالطرق التقليدية، مما يشكل تهديدًا خطيرًا على البيئة. تغطي الدراسة الجوانب النظرية للامتزاز بالإضافة إلى التطبيقات التجريبية، بما في ذلك تحضير المواد، وتوصيفها، وإجراء اختبارات الامتزاز. أظهرت النتائج أن المواد المعدّلة تحسّن بشكل كبير من كفاءة إزالة الهيدروكربونات، خصوصًا عند درجة الحموضة المحايدة. تؤكد هذه النتائج على إمكانية استخدام المواد المسامية في معالجة المياه الصناعية، وتفتح المجال لمزيد من الأبحاث حول تحسين ظروف الامتزاز، وتطوير مواد امتزاز جديدة، ودمج هذه المواد في أنظمة صناعية واسعة النطاق.

General introduction

GENERAL INTRODUCTION

Management and treatment of wastewater from industrial activities constitute a major challenge for the preservation of water resources and pollution control. Nevertheless, in process chains involving hydrocarbons, such as natural gas liquefaction, liquid effluents loaded with hydrocarbons are generated. If not properly treated, these effluents can cause significant damage to receiving environments, such as marine ecosystems, and pose serious risks to human health. Due to their low solubility in water, these hydrocarbons tend to remain on the water surface, forming floating films that prevent light penetration. This disrupts the photosynthesis of aquatic organisms, reduces oxygen production, and alters food chains, thereby impacting biodiversity and marine ecosystems [1].

However, adsorption processes using porous materials represent a simple and effective method to capture hydrocarbons from industrial wastewater. The retention of pollutants on the adsorbent surface allows efficient contaminant removal. Advantages of adsorption include ease of use, relatively low cost, and high effectiveness even at low pollutant concentrations [2]. Despite this, the efficiency depends on several physicochemical factors such as surface area, porosity, chemical composition, surface functional groups, and the nature of the adsorbate [3]. Notably, adsorbent materials, particularly mesoporous materials like MCM-41, have significantly improved performance through modifications such as the incorporation of aluminum and/or grafting of organic molecules.

This thesis work is thus focused on the study of hydrocarbon adsorption present in liquid industrial effluents from a natural gas liquefaction unit. Indeed, treating wastewater in such industrial settings is essential to comply with environmental discharge regulations while ensuring sustainable water resource management [4]. Specifically, we chose to evaluate the adsorption efficiency of hydrocarbons using mesoporous materials from the MCM-41s family under various operating conditions.

The main objective of this research is to optimize the adsorption conditions of hydrocarbons present in industrial liquid effluents by using purely siliceous MCM-41 and aluminum-impregnated Al-MCM-41 mesoporous materials, as well as their derivatives grafted with a new organic molecule. Through a series of experiments, we aim to interpret the interactions between these materials and hydrocarbons, and assess the impact of various parameters on their adsorption capacity. By optimizing ideal conditions and the most effective modification, our goal is to propose efficient solutions for wastewater treatment in industrial facilities.

The overall structure of this thesis, following a GENERAL INTRODUCTION, is divided into two parts:

1- A theoretical part, consisting of:

CHAPTER I: Presentation of the liquefaction complex;

CHAPTER II: Description of the wastewater treatment unit;

CHAPTER III: Adsorption and adsorbents.

2- A practical part, including:

CHAPTER IV: Experimental procedures;

CHAPTER V: Results and discussions.

Finally, all results are compiled in a GENERAL CONCLUSION to conclude this thesis work.

Bibliographic references

[1] N. Ali, M.H. Khan, M. Ali, Sidra, S. Ahmad, A. Khan, G. Nabi, F. Ali, M. Bououdina, G.Z. Kyzas, Insight into microplastics in the aquatic ecosystem: Properties, sources, threats and mitigation strategies, Science of The Total Environment 913 (2024) 169489.

[2] W. Ahmad, T. Muhammad, I. Ahmad, M. Khan, S. Nazneen, Adsorption of hydrocarbon pollutants from wastewater using Cu- and Zn-loaded activated carbon derived from waste tires, Environmental Progress & Sustainable Energy 43 (2024) e14360.

[3] J. Lladó, F. López, J.M. Rossell, C. Lao-Luque, R.R. Gil, E. Fuente, B. Rui, Multivariate analysis of pharmaceutical pollutants adsorption in aqueous media with tailored waste-based carbonaceous adsorbent materials and commercial activated carbons, Sustainable Chemistry and Pharmacy 38 (2024) 101453.

[4] Décret exécutif n° 06-141 du 20 Rabie El Aouel 1427 correspondant au 19 avril 2006 définissant les valeurs limites des rejets d'effluents liquides industriels.

CHAPTER I

Presentation of the liquefaction complex

Table of Contents

CHAPTER I Presentation of the liquefaction complex

List of figures

The GL3/Z liquefaction complex is an industrial facility dedicated to the production of liquefied natural gas, integrating several departments and units to ensure process efficiency. Its laboratory, divided into three sections (water, oil, and gas), plays a crucial role in monitoring product and effluent quality. However, managing the wastewater generated by these activities presents a significant environmental challenge, requiring appropriate treatment to minimize its impact and comply with regulatory standards.

I.1. GENERAL DESCRIPTION OF THE LIQUEFACTION COMPLEX

I.1.1. LOCATION

The site is located on the Mediterranean coast at Bethioua (as shown in Figure I.1), east of Arzew, in the Arzew El Djedid industrial port zone.It covers an area of 54.6 hectares [1].
To the east, it is bordered by the existing GPL liquefied petroleum gas (GPL) production plant, GP1Z, while to the west, it adjoins the seawater desalination plant (Kahrama) as well as the natural gas liquefaction plant.

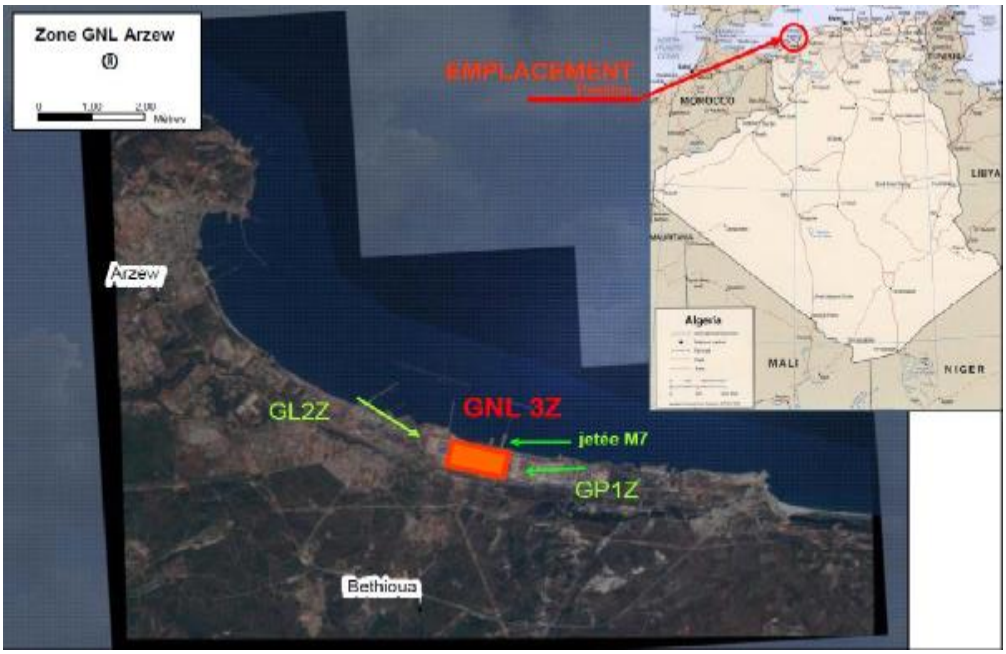

Figure I.1. The geographical location of GL3/Z [2].

I.1.2. PRESENTATION OF THE GL3/Z COMPLEX

The GL3Z complex, located in the industrial zone of Arzew, is a key infrastructure for the production and export of liquefied natural gas (GNL) in Algeria. Commissioned on June 14, 2014, it is the country's first and only mega-train, with an annual production capacity of 4.7 million tons. This strategic site facilitates the delivery of GNL to international markets via

large methane carriers navigating the Mediterranean. Equipped with state-of-the-art technology, the complex carries out essential gas processing stages, including purification, fractionation, and methane liquefaction. This process reduces the gas volume by 600 times, making storage and transport more efficient. GL3Z features two full-containment storage tanks, each with a capacity of 160,000 m^3, ensuring safe storage before export. In addition to GNL, it produces ethane, propane, butane, gasoline, and helium-rich gas, meeting both national and international market demands. Committed to sustainable development, Sonatrach has implemented strategies to reduce the complex's carbon footprint, particularly by progressively minimizing gas flaring. With optimized production capabilities and the expertise of its workforce, GL3Z strengthens Algeria's position as a reliable energy supplier on the global stage [3].

I.1.3. DEPARTMENT DESCRIPTIONS

The organization chart of GLZ3 is shown in Figure I.2.

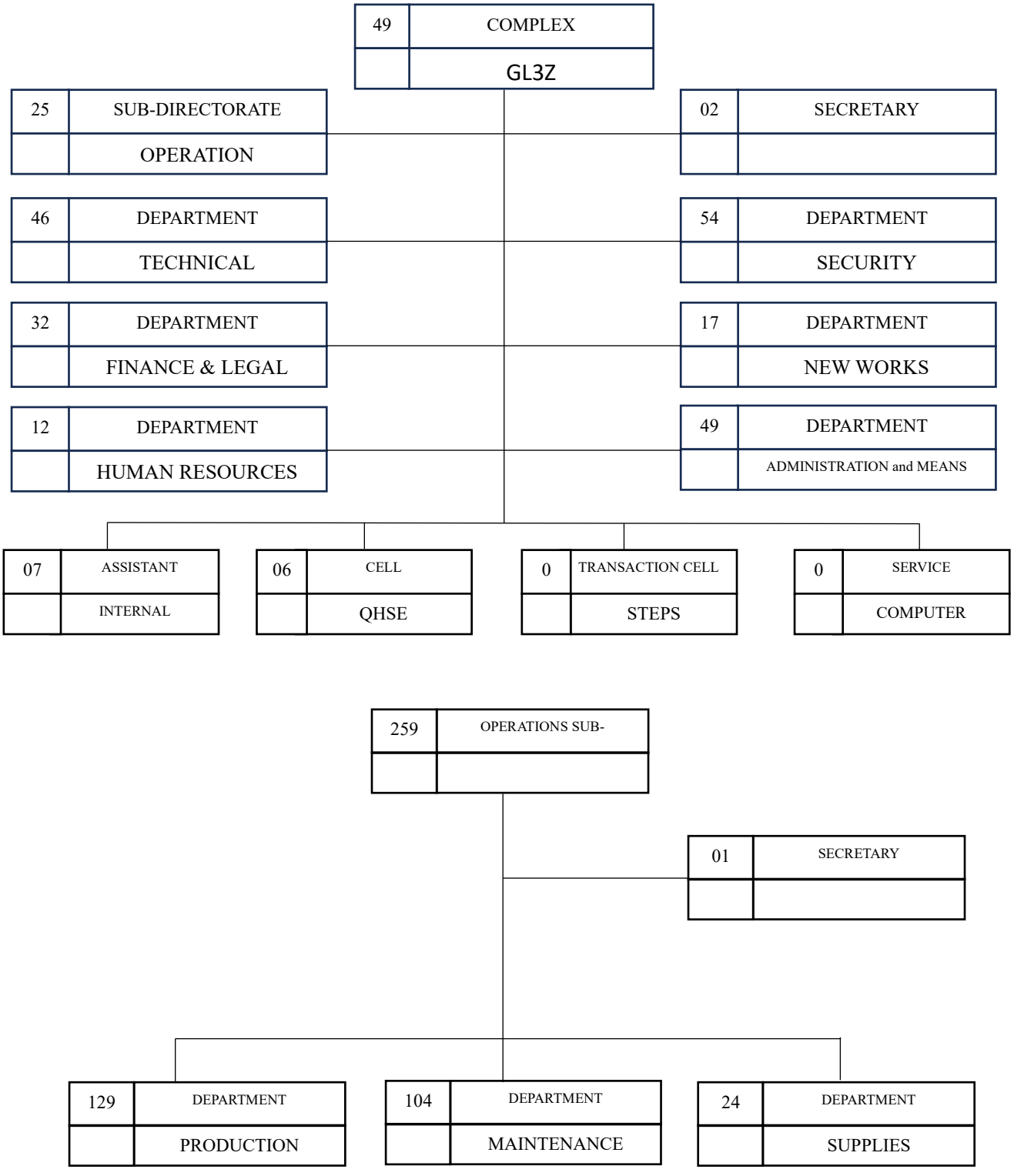

Figure I.2. GL3/Z organization chart [4].

I.1.4. GENERAL DESCRIPTION OF THE GNL PROCESS

The choice of process depends on site-specific conditions, feed gas quality and product specification requirements. A standard natural gas treatment process typically involves the following steps:

- Feed gas, from upstream fields, is delivered at high pressure (around 90 bar) via main pipelines.
- The associated condensates are separated and removed.
- The gas pressure is adjusted and maintained in accordance with plant requirements.
- Before its main treatment, the gas undergoes pre-treatment to remove impurities that could interfere with the process or alter the quality of the finished products. These impurities include acid gases and Sulphur compounds (CO_2, H_2S and mercaptans), water and mercury.
- The gas, now dry and non-corrosive, is then cooled using a refrigerant fluid, allowing the heavy hydrocarbons to be separated. The residual gas, mainly composed of methane, contains less than 0.1 mol% pentane and heavier components (C_5+). It is then sent to the cryogenic section, where it is cooled to around -160°C for complete liquefaction.
- The resulting GNL is stored in atmospheric tanks for export by sea.
- The heavier hydrocarbons are fractionated to recover different cuts:
- Ethane is generally reinjected into the gas stream to be liquefied again.
- Propane and butane can either be reintegrated into the process or exported as GPL
- Pentane and heavier fractions are exported as petrol.
- The operation of the process units relies on a number of essential support utilities, including:
- Fuel gas from the process streams, used to generate electricity.
- Cooling agents (water or air).
- Heating agents (steam or thermal oil).
- Various auxiliary services such as service air, instrument air and nitrogen.

A block diagram (Figure 3) illustrates the general organization of an GNL plant, including the main processing units and the utilities required for their proper operation [2].

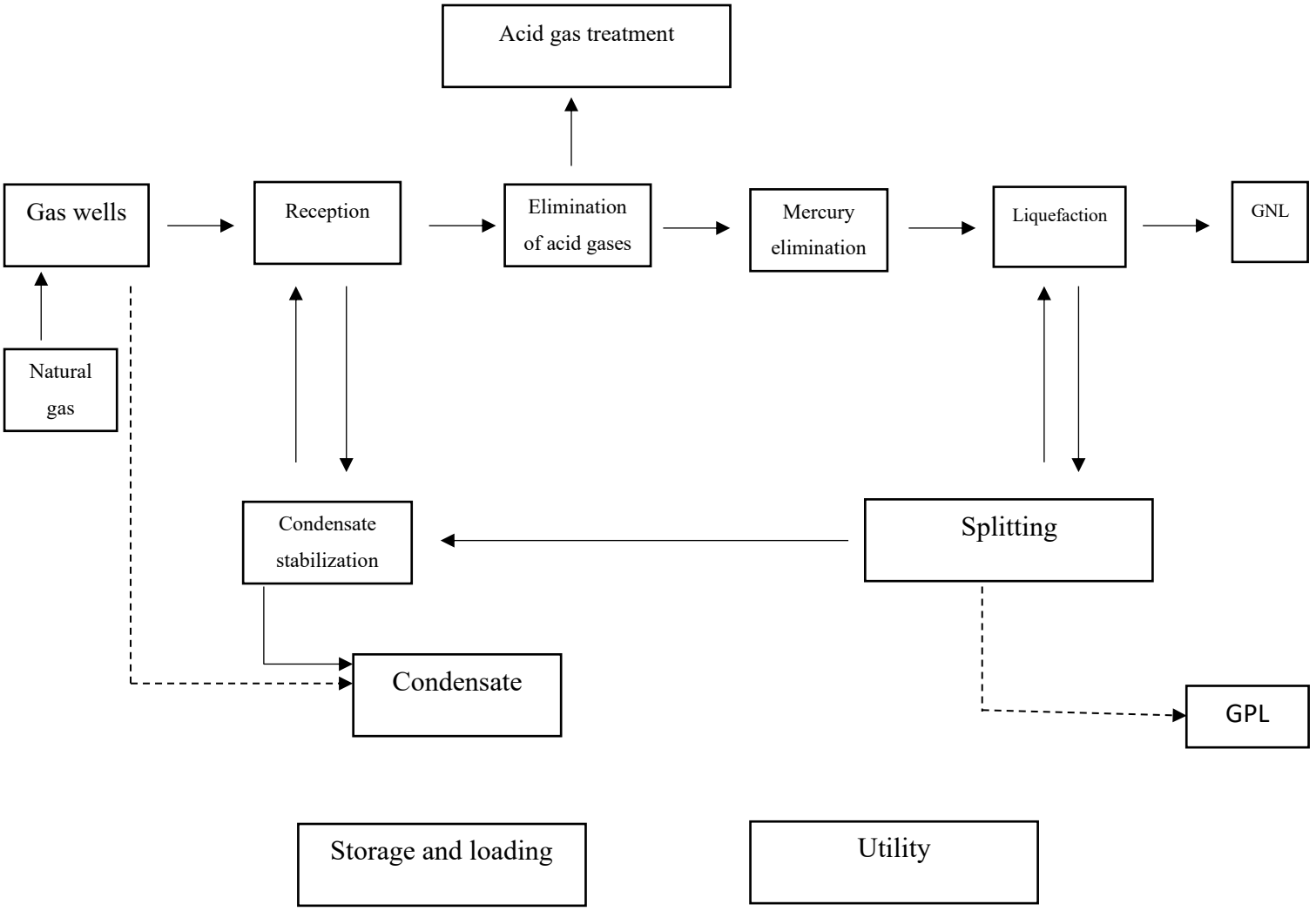

Figure I.3. General Functional Diagram of GNL [2].

I.1.5. DESCRIPTON OF COMPLEX UNITS

The overall functional diagram of the GNL/3Z plant illustrates the main process units, highlighting the main stream flow rates and key connections between the different sections of the plant. It consists of a process train, associated utilities, and an off-site installation. The process train includes a feed gas compressor, a mercury removal section, a CO_2 removal unit licensed by BASF, a dehydration system, a GNL recovery and fractionation unit, and a dedicated propane refrigeration cycle. It also features a liquefaction and refrigeration section (C3SPLIT MR licensed by APCI). The utilities and off-site installations encompass power generation, GNL and GPL storage and loading onto cargo ships, as well as various services such as hot oil, cooling water, service and instrument air, nitrogen, fuel gas, flares, wastewater treatment, service and potable water, diesel, and refrigerant and gasoline storage.

The entire process is carried out within these operational units [4]:

- Unit 11: Feed Gas Treatment
- Unit 12: Acid Gas Removal
- Unit 13: Gas Dehydration
- Unit 14: Train 1 Fuel Gas System
- Unit 15: Liquefaction
- Unit 16: Refrigeration
- Unit 17: LNG Recovery and Fractionation
- Unit 18: Hot Oil System
- Unit 19: Cooling Water System

Utility Zone Units

- Unit 01: Inlet Facilities
- Unit 02: Amine Solvent Storage
- Unit 08: Hot Oil Storage
- Unit 51: Power Generation
- Unit 53: Backup Diesel Generator System
- Unit 55: Common Fuel Gas System
- Unit 56: Service Air and Instrument Air System
- Unit 57: Nitrogen System
- Unit 58: Potable Water Circuit
- Unit 59: Service Water and Demineralized Water System
- Unit 64: Wastewater and Effluent System

Off-Site, Flare, and Jetty Area Units

- Unit 71: LNG Storage and Loading
- Unit 72: LPG Storage and Loading
- Unit 73: Refrigerant Storage System
- Unit 75: Flare System
- Unit 76: Gasoline Storage System

Fire Protection Zone Units

- Unit 63: Fire Water System
- Unit 77: Firefighting System

I.2. LABORATORY SERVICE DESCRIPTION

The GL3/Z laboratory comprises 3 different sections:

- Water section
- Oils section
- Gas section.

In the following part, we are going to deeply describe only the liquefaction section that have a direct link with our thesis work.

I.2.1. WATER SECTION

I.2.1.1. Description of equipment used for water analysis

- pH Meter

Principle:

The pH can be measured using a pH meter. This measurement is based on a potentiometric technique that relies on the change in potential difference between two electrodes. Consequently, a pH meter consists of two electrodes: one has a known (or reference) potential, while the other (the indicator electrode) has a variable potential [5].
pH is a number that indicates the acidity of a solution.

Figure I.4. Image of the used pH meter.

- UV-VISIBLE spectrophotometer:

The UV-VISIBLE spectrophotometer is used to determine the concentrations of various metals present in water.

The principle of this technique is based on the interaction of light with the sample to be analyzed. A part of the incident beam is absorbed, another is reflected, and another is transmitted by the sample [6].

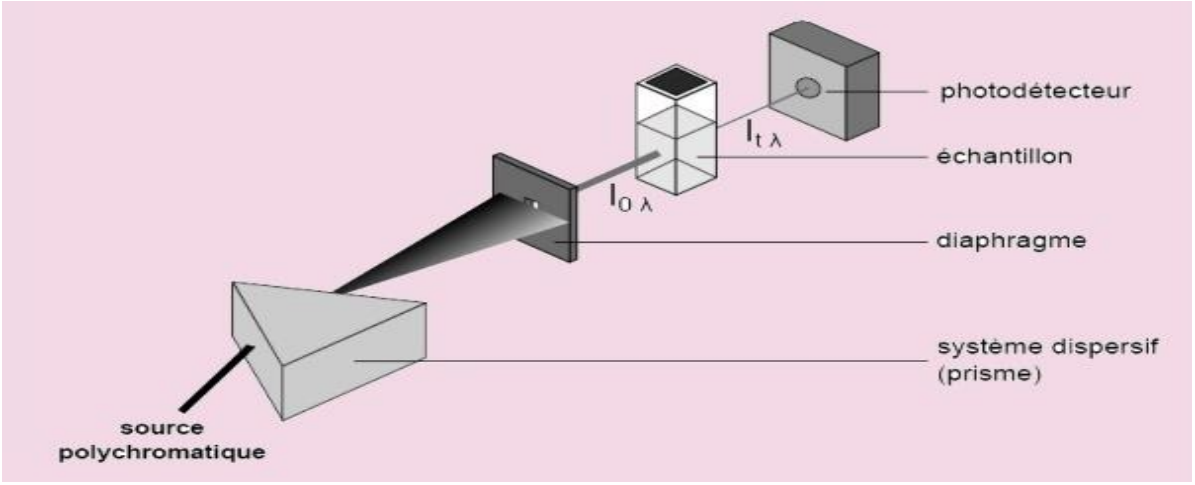

Figure I.5. Principle of a UV-VISIBLE spectrometer [7].

- conductivity meter:

Conductivity is one of the methods used to validate physicochemical water analysis.

Contrasts in measured conductivity within a given environment can help identify pollution, mixing zones, infiltration, corrosion, and other factors.

Conductivity is also temperature-dependent, increasing as temperature rises. It is commonly used to assess the concentration of dissolved salts in water [8,9].

Figure I.6. conductivity meter.

- foaming test:

Evaluation using the MDEA (Methyl Diethanolamine) foaming test is essential to determine the foam formation tendency of amine solutions used for CO_2 absorption in natural gas extraction processes.

- oils and fats (Horiba):

Using this method, the concentration of oils, fats, and total hydrocarbons in oily water is measured in milligrams per liter (mg/L).

Solvent S-316 is used to extract oils, greases, and total hydrocarbons dissolved in water (such as wastewater or oily water).

After extraction, the solvent phase is separated and transferred to the measurement cell of the HORIBA infrared analyzer.

Both qualitative and quantitative analyses of the substances are performed using the infrared (IR) absorption spectrum, which reflects the molecular structure of the compounds [10,11].

Figure I.7. Analyzer for oil and fat content in water.

- Chemical Oxygen Demand (DCO):

Chemical Oxygen Demand (DCO), which refers to the volume of oxygen required for the biological oxidation of biodegradable organic matter, or TSS (Total Suspended Solids).

DCO is determined through reactor digestion and chemical oxidation of organic matter using a strong oxidant (potassium dichromate) [12].

Figure I.8. HACH LANGE LT 200 thermoreactor used for COD analysis.

- Biological oxygen demand DBO_5:

BOD5 (Biochemical Oxygen Demand over 5 days) indicates the amount of oxygen needed by microorganisms to break down the total organic matter in a water sample, kept at 20°C and in darkness, over a 5-day period.

To determine the BOD5, the oxygen concentration of the water sample is measured initially. After 5 days, the measurement is repeated. The BOD5 is the difference between the two oxygen concentrations recorded [13].

Figure I.9. The DBO incubator.

- Dissolved oxygen analyzer:

A dissolved oxygen analyzer is a specialized device used to measure the concentration of oxygen dissolved in a liquid. This measurement is critical for monitoring water quality, ensuring process efficiency [14].

The oximeter, equipped with appropriate oxygen probes, allows the measurement of:

- Oxygen content (mg/L)
- Oxygen saturation index (%)
- Oxygen partial pressure (mbar)

I.3. ENVIRONMENTAL ISSUES RELATED TO WASTERWATER MANAGEMENT

Wastewater management is a crucial aspect of environmental protection, as improper handling can lead to severe ecological and human health issues. Industrial and domestic wastewater

often contains a variety of pollutants, including heavy metals, organic compounds, and pathogenic microorganisms, which can degrade water quality and disrupt aquatic ecosystems [15].

- Water Pollution and Ecosystem Disruption

One of the major environmental risks associated with wastewater discharge is water pollution. Contaminants in wastewater can lead to eutrophication, where excessive nutrients promote the overgrowth of algae, reducing oxygen levels and harming aquatic life. Toxic substances such as heavy metals and hydrocarbons can accumulate in aquatic organisms, affecting biodiversity and potentially entering the food chain [16].

- Impact on Human Health

Poor wastewater management can expose communities to waterborne diseases such as cholera, dysentery, and hepatitis. Pollutants like lead and mercury, commonly found in industrial effluents, can have long-term health effects, including neurological disorders and developmental issues in children [17].

- Soil and Groundwater Contamination

Unregulated wastewater disposal can lead to the infiltration of harmful chemicals into soil and groundwater reserves. This contamination not only affects drinking water supplies but also reduces soil fertility and agricultural productivity, posing a risk to food security [18].

- Climate Change Considerations

Wastewater treatment processes contribute to greenhouse gas emissions, particularly methane and nitrous oxide, which have a significant impact on global warming. The adoption of sustainable treatment technologies, such as anaerobic digestion and biofiltration, can help reduce these emissions while improving energy efficiency [19].

- Regulatory and Technological Solutions

To mitigate these environmental risks, stringent regulations and advanced treatment technologies are required. Improved wastewater treatment infrastructure, stricter discharge limits, and sustainable practices such as water recycling can play a crucial role in reducing environmental impact [20].

I.4. CONCLUSION

In conclusion, this chapter highlights the crucial role played by liquefaction plants in GNL production, while underlining the importance of laboratory services in ensuring product quality and compliance with international standards. It also highlights the environmental issues associated with their operation, in particular wastewater management.

Bibliographic references

[1] H. El M., Étude du système de liquéfaction du gaz naturel GNL3/Z, Mémoire de Master, Université Akli Mohand Oulhadj de Bouira, 2022.

[2] S. Zentici et S. Bennama, Méthodes proposées expérimentales et théoriques de la récupération et la réduction de BOG du bac de butane au niveau du complexe GNL3/Z, Mémoire de Master, Univ. Abdelhamid Ibn Badis Mostaganem, Département de Génie des Procédés, 2020.

[3] F. Zafane, "Complexe de liquéfaction de gaz GL3Z de Bethioua (Oran) : la zone industrielle qui place Sonatrach parmi les leaders mondiaux de l'industrie du gaz," INFO, 14 février 2024.

[4] K. Hiba et H. Goumidi, Dysfonctionnement de la section de réfrigération au niveau de l'unité 72, Mémoire de Master, Université Abdelhamid Ibn Badis – Mostaganem, 2019.

[5] A. Djafer et D. Abbassi, Étude et modélisation d'un capteur de pH à base de transistor à effet de champ, Mémoire de Master, Université 8 Mai 1945 – Guelma, 2020.

[6] A. Hafdallah, Dépôt et caractérisation des électrodes en couches minces transparentes et conductrices, Thèse de doctorat, Université des Frères Mentouri de Constantine, 2016.

[7] A. Eloi, "Introduction à la spectroscopie UV-Visible," CultureSciences-Chimie, ENS Éduscol, 15 septembre 2012.

[8] M. B. Pescod, Wastewater Treatment and Use in Agriculture, FAO Irrigation and Drainage Paper 47, Food and Agriculture Organization, 1985.

[9] J. Rodier, L'analyse de l'eau : eaux naturelles, eaux résiduaires, eau de mer, 6e éd., Paris : Dunod, 1984.

[10] SONATRACH, Analyse des huiles-graisses dans les eaux huileuses, 2016.

[11] B. Tahiri, Contrôle de la qualité des eaux usées : Cas de la station d'épuration (STEP) du complexe GPI/Z de Béthioua (région d'Arzew), Mémoire de Master, Université d'Oran 2 Mohamed Ben Ahmed, 2023.

[12] I. Pásztor, P. Thury, et J. Pulai, "Chemical oxygen demand fractions of municipal wastewater for modeling of wastewater treatment," International Journal of Environmental Science and Technology, 2009.

[13] H. Froissard, Mesure de la demande biologique en oxygène (DBO5), Sciences de la Vie et de la Terre – Académie de Lyon, 2008.

[14] Tomarok Engineering, Dissolved Oxygen Analyzers.

[15] Natural Resources Defense Council, Water Pollution: Everything You Need to Know.

[16] C. Takam, "Assainissement des eaux usées et risques socio-sanitaires et environnementaux en zones d'habitat planifié de Yaoundé (Cameroun)," VertigO - la revue électronique en sciences de l'environnement, vol. 8, no. 3, 2007.

[17] S. Badenhorst, "The effects of sewage pollution on the environment and how to prevent it," Calcamite, 26 février 2024.

[18] S. Ben Kouider et S. Nechadi, Traitement des eaux usées par procédé boues activées : Cas d'étude STEP Beni Mered, Mémoire de fin d'études, Université Saad Dahlab – Blida 1, 2024.

[19] A. Mehammedia, Étude de la performance d'une station d'épuration des eaux usées urbaines : Cas de la STEP de Bouchegouf, Mémoire de Master, Université 8 Mai 1945 – Guelma, 2022.

[20] M. Saadi et F. A. Lahmar, Évaluation de l'efficacité de la station d'épuration de Guelma (Nord-Est Algérie), Mémoire de Master, Université Badji Mokhtar – Annaba, 2018.

CHAPTER II

Description of wastewater treatment plant

Table of Contents

CHAPTER II. DESCRIPTION OF WASTEWATER TREATMENT PLANT

List of figures

List of tables

Hydrocarbon contamination of industrial wastewater is a significant environmental concern for industrial plants. The management of this pollution is often linked to the performance of wastewater treatment plants. In this segment, we have detailed the operation of the water treatment unit (64), highlighting the physical, chemical, or biological methods employed. These methods have certain limitations, particularly in terms of complete hydrocarbon removal. This chapter also looks at technological options and recent innovations likely to improve treatment performance, while ensuring sustainability and compliance with regulatory standards.

II.1. OPERATION OF THE CURRENT TREATMENT UNIT

II.1.1. DEFINITION OF WASTEWATER

Wastewater refers to all waters that have been contaminated as a result of human activities, whether directly through domestic or economic use (industrial, artisanal, agricultural, etc.), or indirectly through urban runoff. This water must undergo physical and/or chemical treatment before being discharged into the environment [1].

II.1.2. ORIGIN OF WASTEWATER

Wastewater mainly originates from the following sources:

The physicochemical and bacteriological degradation of initially clean water intended for consumption.

Human activities, whether domestic, industrial, or agricultural.

Water runoff, depending on the nature of the pollutants encountered along its path [2].

II.1.3. DIFFERENT WASTEWATERS

II.1.3.1. Domestic Wastewater

Domestic wastewater consists of two main categories:

Greywater: Originating from kitchens, bathrooms, and laundry, it contains detergents, fats, organic residues, and other pollutants.

Blackwater: Coming from toilets, it is rich in fecal matter and urine.

Urban wastewater, on the other hand, is discharged from collective facilities such as hospitals, schools, commercial buildings, and residential areas [2].

II.1.3.2. Industrial Wastewater

Unlike domestic wastewater, industrial wastewater varies greatly in composition depending on the type of industry. In addition to organic, nitrogenous, or phosphorus-based pollutants, it may contain various chemical substances of organic or metallic origin. Depending on the sector, it can include:

- Fats (e.g., from the agri-food industry or animal rendering).
- Hydrocarbons (from refineries).
- Heavy metals (from metallurgy or surface treatment processes).
- Acids, bases, and other chemicals (from chemical industries or tanneries).
- Hot water (from cooling circuits in thermal power plants).
- Radioactive substances (from nuclear plants or radioactive waste treatment).

Before being discharged into sewer systems, industrial wastewater must undergo appropriate treatment. It may only be mixed with domestic wastewater if it no longer poses a risk to collection infrastructure and does not interfere with the proper functioning of wastewater treatment plants [2].

II.1.3.3. Stormwater

Stormwater includes rainwater, surface cleaning water, and drainage water. As it flows, it collects various mineral and organic wastes from urban and natural surfaces [3].

II.1.3.4. Agricultural Wastewater

Agriculture is a significant source of water pollution, mainly due to the use of fertilizers and pesticides. It is the leading cause of diffuse pollution. Runoff from cultivated lands carries nitrates and phosphates (either in ionic form or in such high concentrations) that they are not absorbed by the soil or plants. These nutrients then reach shallow groundwater and surface water bodies, leading to excessive enrichment in nitrogen and phosphorus compounds [2].

II.1.4. TYPES OF WASTEWATERS TREATMENT

The various wastewater treatment processes are presented in the typical order followed in a conventional treatment chain:

- Pre-treatment: screening and straining, grit removal, and oil removal.
- Primary treatment: sedimentation.

- Secondary treatment (biological): biological purification of organic matter.
- Tertiary treatment: removal of nitrogen and phosphorus, disinfection, and sludge treatment [3].

II.1.4.1. Pre-treatment

Screening and Straining

Screening and straining are used to remove large solid waste from the water, such as wipes, rags, and materials like plastic or wood. Since these elements do not naturally decompose over time, they must be removed mechanically rather than through biological or physic-chemical treatment [4].

Grit and Oil Removal

Sediments are removed through sedimentation, while fats and oils are separated by injecting microbubbles of air that help them rise to the surface. Once at the surface, they are skimmed off using a scraping system. The waste collected during this stage may undergo further treatment and be reused as organic or sedimentary material [4].

II.1.4.2. Primary Treatment

This stage mainly involves a sedimentation process that removes up to 60% of suspended solids (SS) and approximately one-third of the incoming five-day biochemical oxygen demand (BOD_5) from the wastewater [5].

Sedimentation

Primary sedimentation promotes the settling of suspended solids by gravity, resulting in sludge accumulation at the bottom of the tanks [6]. This sludge is then extracted using a pumping system. The process takes place in circular sedimentation tanks equipped with scrapers or in lamella settlers [5].

II.1.4.3. Secondary Treatment (Biological)

The main goal of biological treatment is to eliminate organic compounds such as sugars, fats, and proteins. These substances are harmful to the aquatic environment because their breakdown consumes dissolved oxygen, which is essential for the survival of aquatic life.
The concentration of organic pollutants is typically measured by the BOD_5 (Biochemical Oxygen Demand over five days) or the COD (Chemical Oxygen Demand).

The microorganisms responsible for breaking down organic matter are heterotrophic bacteria. To speed up the degradation process, oxygen must be artificially supplied to the wastewater to stimulate bacterial activity [5].

II.1.4.4. Tertiary Treatment

At the end of secondary treatment, treated wastewater is typically discharged into the natural environment. However, in some cases, additional treatment – also known as polishing – is necessary. This process aims either to enable the reuse of water for industrial or agricultural purposes or to protect sensitive receiving environments based on specific intended uses.

When the water is to be discharged into sensitive areas, such as bathing zones or shellfish farming areas, disinfection is essential. Conventional treatment does not eliminate bacteriological pollution. This disinfection is usually carried out by adding chlorine in a contact tank or by using ultraviolet (UV) light treatment.

Furthermore, the removal of nitrogen and phosphorus is a complementary treatment that has become increasingly common in wastewater treatment plants due to its critical role in preventing eutrophication of aquatic environments [5].

Sludge Treatment

Sludge from various treatment stages undergoes a specific treatment process. Depending on their final destination, these treatments primarily aim to reduce the volume of the sludge, thus facilitating its transport, storage, or valorization [5].

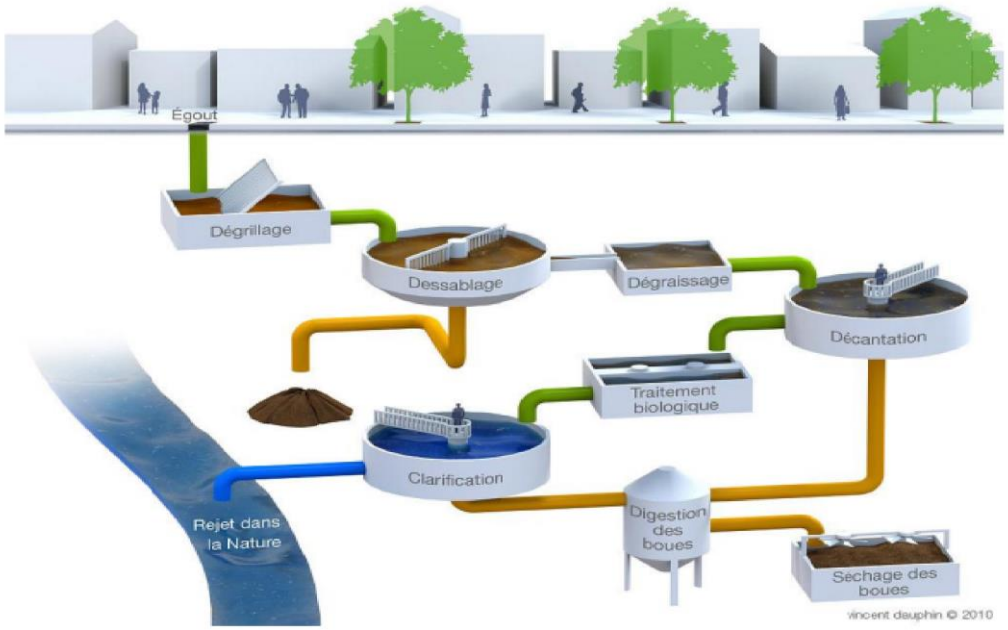

Figure II.1. Diagram of a Wastewater Treatment Plant [7].

II.1.5. GENERAL OVERVIEW OF UNIT 64

Unit 64 is dedicated to the treatment of effluent and wastewater from washing, run-off, sanitary sewers, and drains polluted by hydrocarbons of either accidental or systemic in origin. After undergoing a treatment process, this water is discharged into the sea only when it complies with current environmental standards, thus guaranteeing the protection of marine ecosystems.

Table II.1. Industrial Liquid Effluent Discharge Limits [8].

Parameter	**Unites**	**Values max**
Temperature	°C	30
Ph		5,5-8,5
Matières in suspension	mg/l	25
DBO_5	mg/l	25
DCO	mg/l	100

II.1.6. DESCRIBE THE STRUCTURE AND ROLE OF THE TREATEMENT UNIT

II.1.6.1. Role of Unit 64

- Ensure efficient wastewater treatment.
- Contribute to environmental protection.
- Protect public health by reducing effluent-related risks [3].

II.1.6.2. Structure description unit 64

Figure II.2. Water treatment plant (unit 64).

The Effluent and Wastewater Treatment System (Unit 64) comprises the following equipment:

II.1.6.3. Sanitary sewage system

- 64-ML01 Biological Treatment Unit.
- 64-ML03 Lifting Station for Sanitary, Main Control Room and Laboratory.
- 64-ML04 Maintenance workshop for sanitary lifting stations.
- 64-ML05 Sanitary Lifting Station for Administration Area.
- 64-ML06 Security Building Sanitary Lifting Station.
- 64-CV28 Septic tank.

II.1.6.4. Drainage system for water continuously and accidentally contaminated with oil

- 64-ML02 CPI Separator Assembly.
- 64-MD02 Regeneration water expansion tank.
- 64-CV02 Liquid Discharge Retention Basin.
- 64-MJ02-A/B Contaminated water recycling pumps.
- 64-MF01 Skimmed oil tank [8].

II.1.7. OIL-CONTAMINATED WATER DRAINAGE SYSTEM

The main sources of hydrocarbon-polluted water are the maintenance areas, the LNG plant's retention areas and various items of equipment such as pump bases, compressors, lubrication systems and diesel loading/unloading areas. This water is channeled to pits located close to the emission sites, and then collected by an underground sewer system. Run-off water from rain, cleaning or incidents (such as fires) can also be contaminated, and is directed by gravity to the 64-CV02 retention basin. This device is based on the concept of the flushing effect, managing only the first volume of run-off water, known for its high pollutant content, while the surplus is discharged without any intervention if deemed clean.

The basin also receives wastewater from pit 75-CV01 (flare zone) and separation tank 13-MD03, after passing through tank 64-MD02. A separator at the basin inlet eliminates suspended solids and directs the flows to a bypass column. The first inch of water collected is then pumped to the CPI separator (64-ML02) for treatment. If the quality criteria set by Algerian regulations are not met, this water can be recycled back into the basin. An automatic sampler monitors the quality of discharge from the CPI system.

The CPI separator extracts oil based on the difference in density between water (continuous phase), oil (dispersed phase) and suspended substances. The unit is equipped with parallel plates that encourage gravitational separation, facilitating the ascent of oil droplets to the surface by coalescence and collection. After filtering, the clarified water is conveyed to the

sea discharge via a manual valve, which is usually open. However, this valve must be closed as soon as the discharge quality no longer meets current environmental standards [8].

II.2. LIMITATIONS OF EXISTING TECHNOLOGIES FOR HYDROCARBON REMOVAL

II.2.1. DEFINITION HYDROCARBONS

Hydrocarbons are usually represented by the chemical formula CnHm, where n and m are positive integers. Depending on temperature and pressure, these substances can exist as solids (such as kerosenes), liquids (such as gasoline, petroleum, etc.) or gases (such as methane, butane, etc.). In addition to carbon and hydrogen atoms, some hydrocarbons may contain elements such as oxygen, nitrogen and sulfur, as well as traces of metals such as nickel and vanadium [9].

Petroleum hydrocarbons are highly harmful organic pollutants due to their long persistence, wide distribution, complex composition and toxicity. Aliphatic and polycyclic aromatic hydrocarbons are the most commonly encountered [10].

II.2.2. LIMITATIONS OF CONVENTIONAL TREATEMENT METHODS

II.2.2.1. Activated carbon adsorption

- Limited Effectiveness Against Certain Contaminants: For example, it is ineffective in eliminating inorganic contaminants like certain salts or heavy metals (like lead and arsenic).
- Saturation and Replacement: Activated carbon may eventually become saturated with impurities that have been adsorbed, which will reduce its efficacy. To maintain optimal performance, regular replacement or reactivation is required. High replacement costs.
- Potential for Microbial Growth: Activated carbon filters have the potential to develop into microbial breeding grounds if improperly managed.
- Expensive replacement expenses [11].

II.2.2.2. Chemical oxidation

- High costs of running Chemical oxidants, such as persulfate, hydrogen peroxide, and ozone, are costly [12].

- Importance of specific conditions (pH, temperature, catalyst)

II.2.2.3. Decanting and gravity separation (API, CPI)

- they are ineffective with tiny oil droplets or emulsified oil, and they need a long retention period to separate well.
- Compared to other approaches, the concentration of effluent oil is higher.
- Expensive oil/bottom scrapers required that are maintenance intensive [13].

II.2.2.4. Photocatalysis with TiO_2

- Catalyst difficult to recover and reuse [14].
- Potentially hazardous by-products: imperfect decomposition of hydrocarbons may give rise to several intermediate by-products. Such as aldehydes or carboxylic acids Potentially hazardous by-products: imperfect decomposition of hydrocarbons may give rise to several intermediate by-products. Such as aldehydes or carboxylic acids [15].

II.2.2.5. Bioremediation

- Environmental factors such as temperature, pH, humidity and the presence of nutrients have an impact on the activity of microbes, which can slow down or hinder hydrocarbon decomposition [16].
- The partial degradation of complex compounds such as polycyclic aromatic hydrocarbons (PAHs), which are often resistant to biodegradation, can lead to the generation of potentially toxic by-products [17].

II.2.2.6. Ozonation

- Ozone production costs (process equipment) are high [18].
- The need to produce ozone on site.
- The efficiency of the technology can be reduced by the presence of substances that react with the oxidant (iron, manganese, carbonates, etc.) [19].

II.3. TECHNOLOGICAL ALTERNATIVES AND POSSIBLE INNOVATION

The removal of hydrocarbons from industrial waste8ater remains a significant challenge due to their complex chemical structures and low biodegradability. To address the limitations of

conventional treatment methods, several innovative technologies have been developed to enhance efficiency, reduce costs, and minimize environmental impact.

II.3.1. ADVANCED OXIDATION PROCESSES (AOPS)

Advanced Oxidation Processes (AOPs) involve the generation of highly reactive hydroxyl radicals capable of degrading a wide range of organic pollutants, including hydrocarbons. Techniques such as the Fenton reaction, photo-Fenton, ozonation, and photocatalysis have demonstrated effectiveness in oxidizing hydrocarbons into less harmful substances. However, challenges remain in scaling these processes for industrial applications and ensuring consistent performance across varying wastewater compositions [20].

II.3.2. ADSORPTION USING MESOPOROUS MATERIALS

Adsorption is one of the most promising techniques for removing hydrocarbons from industrial effluents. Mesoporous materials such as MCM-41 and AlMCM-41 possess high specific surface areas, uniform pore size distributions, and functionalizable surfaces, making them ideal for adsorbing hydrophobic organic molecules [21].

II.3.3. ADVANCED BIOREMEDIATION

Bioremediation leverages the metabolic capabilities of microorganisms to degrade hydrocarbons. Strategies such as bioaugmentation (introducing specialized microbial strains) and biostimulation (adding nutrients to stimulate indigenous microbes) have been employed to enhance degradation rates. These methods are environmentally friendly and cost-effective, though their efficiency can be influenced by environmental factors and the specific composition of the wastewater [22].

II.3.4. HYBRID TECHNOLOGIES

Combining different treatment methods can overcome the limitations of individual processes. Hybrid systems, such as integrating adsorption with bioremediation or coupling AOPs with membrane filtration, have shown improved performance in treating complex effluents. These integrated approaches can enhance pollutant removal efficiency and offer greater flexibility in handling diverse wastewater streams [23].

II.4. CONCLUSION

Following an analysis of the current wastewater treatment plant, this chapter shows that it generally operates efficiently. However, it has its limitations when faced with the complexity and variety of hydrocarbon-based pollutants (high organic loads or presence of heavy hydrocarbons). Nevertheless, alternative approaches have been considered, such as advanced oxidation, specific bioremediation or the use of advanced sorbents. These significantly increase treatment efficiency and guarantee superior environmental protection.

Bibliographic references

[1] Pollutec, "Les eaux usées : qu'est-ce que c'est et comment sont-elles traitées ?", Learn & Connect, 12 janvier 2022.

[2] A. Mehammedia et K. Touati Tliba, Évaluation de l'efficacité de la station d'épuration des eaux usées (STEP) de Guelma, Mémoire de Master, Université 8 Mai 1945 Guelma, 2020.

[3] M. Saadi et F. A. E. Lahmar, Évaluation de l'efficacité de la station d'épuration de Guelma (Nord-Est Algérie), Mémoire de Master, Université Badji Mokhtar – Annaba, 2018.

[4] JC France Industrie, "Les différentes étapes du traitement des eaux", 22 décembre 2021.

[5] K. Sadaoui, Dimensionnement du système photovoltaïque appliqué à une station d'épuration des eaux usées, Mémoire de Magister, Université Kasdi Merbah Ouargla, 2017.

[6] H. Labbaci et T. Boumenkar, Analyse des anomalies et redimensionnement de la STEP de la Wilaya de Skikda, Mémoire de Master, Université Badji Mokhtar Annaba, 2019.

[7] A. Chahed, Étude comparative entre deux méthodes de calcul (GDF et Belge) pour la détermination de l'énergie livrée au terminal GL2/Z, Mémoire de Master, Université Abdelhamid Ibn Badis Mostaganem, 2016.

[8] Sonatrach, Description des Utilités – Unité 64 : Système des Effluents et Eaux Usées, Doc. No. 64-ZA-E-86007, Rev. 1, Projet GNL-3Z, Arzew, Algérie, 27 janvier 2011. Snamprogetti, Chiyoda Corporation, Saipem.

[9] H. Hassaine, Biodégradation des hydrocarbures (pétrole brut et kérosène) par la microflore microbienne des eaux de la région de Skikda, Thèse de doctorat, Université Badji Mokhtar – Annaba, 2016.

[10] H. Bekenniche, Exploration de la biodiversité microbienne dans des sites pollués par les hydrocarbures en Algérie : Biologie moléculaire et génétique des microorganismes, Thèse de doctorat, Université Abdelhamid Ibn Badis – Mostaganem, 2021, pp. 5–171.

[11] J. Smith, "The Role of Activated Carbon in Water Treatment: Benefits and Limitations," LinkedIn, 12 octobre 2023.

[12] Beltrán, "Ozone Reaction Kinetics for Water and Wastewater Systems," 2003.

[13] American Water Chemicals, Inc., Corrugated Plate Separators Package, American Water Chemicals, 2025.

[14] H. Dong, G. Zeng, L. Tang, C. Fan, C. Zhang, X. He, et Y. He, "An overview on limitations of TiO_2-based particles for photocatalytic degradation of organic pollutants and the corresponding countermeasures," Water Research, vol. 79, pp. 128–146, 2015.

[15] L. Mohammadi, A. Rahdar, E. Bazrafshan, H. Dahmardeh, M. A. B. H. Susan, et G. Z. Kyzas, "Petroleum Hydrocarbon Removal from Wastewaters: A Review," Processes, vol. 8, no. 4, p. 447, 2020.

[16] N. M. Jabbar, S. M. Alardhi, A. K. Mohammed, I. K. Salih, et T. M. Albayati, "Challenges in the implementation of bioremediation processes in petroleum-contaminated soils: A review," Environmental Nanotechnology, Monitoring & Management, vol. 18, p. 100694, 2022.

[17] B. Thapa, S. Ajay, et R. P. Yadav, "A review on bioremediation of petroleum hydrocarbon contaminants in soil," Kathmandu University Journal of Science, Engineering and Technology, vol. 8, no. 1, pp. 164–170, 2012.

[18] U.S. Environmental Protection Agency, Wastewater technology fact sheet: Ozone disinfection, EPA 832-F-99-063, Office of Water, 1999.

[19] Gouvernement du Canada, "Oxydation chimique – Traitement à l'ozone – ex situ," Gestion optimale des sites contaminés (GOST).

[20] U. Hübner, S. Spahr, H. Lutze, A. Wieland, S. Rüting, W. Gernjak, et J. Wenk, "Advanced oxidation processes for water and wastewater treatment – Guidance for systematic future research," Heliyon, vol. 10, no. 9, p. e30402, 2024.

[21] K. R. Kalash et T. M. Albayati, "Remediation of oil refinery wastewater implementing functionalized mesoporous materials MCM-41 in batch and continuous adsorption process," Desalination and Water Treatment, vol. 220, pp. 130–141, 2021.

[22] S. J. Varjani, "Microbial degradation of petroleum hydrocarbons," Bioresource Technology, 2017.

[23] Genesis Water Technologies, Innovations in Industrial Wastewater Treatment: A New Era, 2023.

CHAPTER III

Adsorption and Adsorbent

Table of Contents

CHAPTER III Adsorption and Adsorbent

List of tables

III.1. ADSORPTION PHENOMENON

Adsorption plays a key role in many industrial processes, such as gas separation and purification, as well as wastewater treatment. The interaction between a solid adsorbent and adsorbate molecules in a fluid phase enables the selective capture of certain undesirable compounds. Through adsorption, it is particularly advantageous to capture organic pollutants such as hydrocarbons, which are frequently found in industrial effluents, especially in natural gas liquefaction plants [1].

The textural characteristics of the adsorbent used, along with its surface chemical properties, play a crucial role in the effectiveness of the adsorption process. Mesoporous materials, such as MCM-41 and Al-MCM-41, have demonstrated a high adsorption capacity due to their large specific surface area, pore volume, and ability to interact with organic molecules. Moreover, the grafting of organic compounds onto the surface of these materials further enhances their performance by introducing functional structures that strengthen interactions with the targeted pollutant [2].

This chapter aims to analyze the fundamental principles of adsorption, the various theories governing this phenomenon, and the characteristics of the adsorbent materials used in this study. Particular emphasis will be placed on the essential role of adsorption in the treatment of industrial wastewater using modified mesoporous materials, especially for the removal of hydrocarbons present in the effluents of a natural gas liquefaction plant.

III.1.1. TYPES OF ADSORPTIONS

Adsorption is defined as a phenomenon in which ions or molecules from a fluid phase, known as adsorbates, adhere to the surface of a solid called an adsorbent. This surface phenomenon can occur either reversibly or irreversibly, depending on the affinity between the adsorbate species and the surface of the adsorbent. Adsorption can be classified according to several criteria, but the two main types of adsorptions, as previously mentioned, are chemisorption and physisorption [3,4].

III.1.1.1. Physical Adsorption

This mechanism is based on weak intermolecular forces, such as van der Waals interactions. It occurs at low temperatures and is usually reversible. Physisorption is ideal for applications requiring rapid adsorption and desorption, such as in continuous effluent treatment cycles [5].

III.1.1.2. Chemical Adsorption

This process involves the formation of strong chemical bonds, such as covalent or ionic bonds, between the adsorbent and the adsorbate. Chemisorption is more specific and often occurs at elevated temperatures. This type of adsorption is particularly useful when stronger interactions and prolonged retention are required, as in the case of heterogeneous catalysis [5]. However, mesoporous materials such as the M41S family can promote both types of adsorptions depending on their final chemical composition and/or post-synthesis modification [1,2]. For instance, methyl diethanolamine (MDEA), which has an amphiphilic structure, enhances chemical interactions with various hydrocarbon molecules and the surface of adsorbents.

The characteristics of physisorption and chemisorption are not limited to the strength of interactions between the adsorbent and adsorbate, but also include their thermodynamic properties.

Table III.1. Comparison between physisorption and chemisorption in adsorption processes.

Characteristic	Physisorption	Chemisorption
Nature of interactions	Van der Waals forces (weak interactions)	Strong chemical bonds (covalent or ionic)
Adsorption energy	Low (< 40 kJ/mol)	High (> 40 kJ/mol)
Operating temperature	Low, generally near room temperature	Higher, sometimes required to activate the chemical reaction
Reversibility	Generally reversible	Often irreversible
Process rate	Fast	Relatively slower
Monolayer/Multilayer	Can occur in multilayers	Monolayer only
Specificity	Low specificity (non-selective adsorption)	Highly specific (depends on active sites and the adsorbate)

III.1.2. IMPORTANCE OF ADSORPTION IN INDUSTRIAL WASTEWATER TREATMENT

In industrial wastewater treatment, adsorption plays a crucial role due to its efficiency in removing various contaminants, such as heavy metals, hydrocarbons, and other volatile organic compounds. This process is particularly suitable for managing effluents from industries such as petrochemicals, power generation, and natural gas liquefaction, where toxic and polluting substances are often present in significant quantities [6].

Furthermore, adsorption offers advantages due to its operational flexibility. It is suitable for treating large volumes of contaminated water at high flow rates, while being compatible with a wide range of pollutants. Adsorbent materials have the ability to capture pollutants directly on their surface without requiring additional chemical intermediates, thereby reducing the risk of producing undesirable by-products [7].

Moreover, mesoporous materials, such as the M41S family, are distinguished by their efficiency in pollutant adsorption. Thanks to their mesoporous channel systems and large specific surface areas; they can effectively adsorb pollutants even at very low concentrations [8]. In addition, overall process performance can be enhanced through functionalization methods, such as the grafting of amphiphilic organic molecules like MDEA, which strengthen specific interactions with hydrocarbon molecules, whether polar or non-polar.

In addition, the low solubility of hydrocarbons in water and their tendency to form floating layers on the surface make them difficult to remove by conventional methods such as filtration or precipitation. However, adsorption addresses this issue by selectively capturing pollutants on the surface of the adsorbent, even in diluted systems. This makes it an ideal approach for managing industrial effluents, which are often rich in oils and petroleum derivatives [9].

Furthermore, the adsorption technique offers the advantage of being relatively simple to implement on a large scale. The reuse or regeneration of adsorbent materials, such as mesoporous substances, helps reduce long-term operational costs. Depending on the treatment conditions, adsorbents can be regenerated using techniques such as heating, washing, or pressure changes, without resorting to complex processes [10]. By using advanced materials such as MCM-41 and Al-MCM-41, it is possible to optimize the process and achieve higher performance across various industrial environments.

III.2. THEORIES OF ADSORPTION

The adsorption process is complex and influenced by various physical and chemical parameters, such as the nature of the adsorbent, the characteristics of the adsorbates, and operational conditions including temperature, pressure, concentration, and contact time. To better understand and represent this phenomenon, two essential theoretical components are frequently examined: adsorption isotherms and adsorption kinetics. These theories are used to predict the behavior of adsorbents under various conditions and to improve industrial processes [11].

III.2.1. ADSORPTION ISOTHERMS

Adsorption isotherms are graphical mathematical representations that illustrate the distribution of adsorbate molecules between the fluid phase (liquid or gas) and the surface of the adsorbent at a constant temperature. These diagrams play a crucial role in describing the interactions between the adsorbent and the adsorbate, the energy levels of active sites, and in determining the maximum adsorption capacity [12].
The most commonly studied isotherm models are:

III.2.1.1. Langmuir Isotherm

The Langmuir isotherm is based on the idea that adsorption occurs at specific sites on the surface of the adsorbent, known as active sites, and that it takes place in the form of a monolayer. It is also assumed that all sites are identical and that there are no interactions between the adsorbed molecules in this model [13]. The Langmuir isotherm is represented by Equation III.1:

$$q_e = \frac{q_{max} K_L C_e}{1 + K_L C_e} \qquad \text{(Eq.III. 1)}$$

Where:

q_e: the amount adsorbed at equilibrium (mg/g);

q_{max}: the maximum monolayer adsorption capacity (mg/g);

C_e: the equilibrium concentration of the adsorbate (mg/L);

K_L: the Langmuir constant, representing the affinity of the adsorbent for the adsorbate.

This model is particularly suitable for systems where adsorption is chemical (chemisorption) and uniform across the surface of the adsorbent, especially in cases where specific active sites are involved.

III.2.1.2. Freundlich Isotherm

Unlike the Langmuir isotherm, the Freundlich isotherm describes adsorption on heterogeneous surfaces, with multilayer adsorption and the presence of adsorbate–adsorbate interactions. This empirical model is used to describe systems in which adsorption forces vary across different sites [13]. The Freundlich equation is represented by Equation III.2:

$$q_e = K_F C_e^{\frac{1}{n}} \qquad \text{(Eq.III. 2)}$$

Where:

K_F: Freundlich constant, indicating the adsorption capacity;

$\frac{1}{n}$: a parameter indicating the intensity of the adsorption (when n=1, the adsorption is linear).

This model is generally applied to physical adsorption (physisorption), where adsorption occurs more easily at low concentrations and becomes more difficult as concentration increases [14]. It is well suited for describing porous surfaces such as MCM-41 and Al-MCM-41, where the pore distribution can create sites with varying energy levels.

III.2.1.3. Temkin Isotherm

In the Temkin model, adsorption is described by considering that the adsorption energy decreases linearly with increasing surface coverage due to adsorbate–adsorbate interactions. Unlike the Langmuir model, which assumes constant adsorption energy, the Temkin model is suitable for systems where these interactions significantly influence the adsorption process [15]. The Temkin equation is represented by Equation III.3:

$$q_e = B \ln(A_T . C_e) \qquad \text{(Eq.III. 3)}$$

Where:

q_e: Amount adsorbed at equilibrium (mg/g);

C_e: Equilibrium concentration of the adsorbate (mg/L);

A_T: Temkin isotherm equilibrium binding constant (L/mg);

$B = \frac{RT}{b}$: A constant related to the heat of adsorption, where R is the universal gas constant (8.314 J/mol·K), T is the temperature (K), and b is the Temkin constant related to the adsorption energy.

This model is relevant for monolayer adsorption systems with heterogeneous surfaces. In this study, it is applied to analyze the adsorption of hydrocarbons on mesoporous materials, taking into account molecular interactions and the properties of the adsorbent.

III.2.2. ADSORPTION KINETICS

Adsorption kinetics describes the rate at which adsorbate molecules are captured on the surface of the adsorbent over time. It is essential to determine the time required to reach adsorption equilibrium and to optimize operational conditions in industrial processes. Among the various kinetic models used in adsorption studies, the most commonly applied are the pseudo-first-order and pseudo-second-order models [16].

III.2.2.1. Pseudo-First-Order Model

Lagergren proposed this model assuming that the adsorption rate is directly related to the number of available active sites on the surface of the adsorbent [13]. Equation III.4 presents the pseudo-first-order model:

$$\frac{dq_t}{dt} = k_1 (q_e - q_t) \qquad (Eq.\ III.\ 4)$$

Where:

q_t : amount of adsorbate adsorbed at time t (mg/g);

q_e : amount of adsorbate adsorbed at equilibrium (mg/g);

k_1 : pseudo-first-order rate constant (1/min).

This model is used to describe rapid physical adsorption, typically occurring on easily accessible sites, such as the surface of porous materials.

III.2.2.2. Pseudo-Second-Order Model

The pseudo-second-order model, which is based on the assumption that the adsorption rate is determined by the number of unoccupied sites, is generally more suitable for describing chemisorption processes [13]. Equation III.5 illustrates the mathematical representation of the model:

$$\frac{dq_t}{dt} = k_2 (q_e - q_t)^2 \qquad \textit{(Eq. III. 5)}$$

Where:

K_2: pseudo-second-order rate constant (g/mg·min).

This model is frequently applied in systems where chemical interactions are predominant, such as when the adsorbent has been functionalized with an organic molecule to enhance its interactions with hydrocarbon molecules.

It is nonetheless crucial to conduct an analysis of adsorption isotherms and kinetics in order to understand and optimize the performance of adsorbent materials in industrial purification systems. Through these models, it is possible not only to measure the adsorption capacity of materials but also to predict their behavior during the adsorption process under real conditions, thereby improving their efficiency in key operations such as industrial wastewater treatment.

III.2.2.3. Intraparticle Diffusion Model

The intraparticle diffusion model (also known as the Weber–Morris model) is used to determine whether the adsorption process is controlled by the diffusion of adsorbed molecules within the pores of the adsorbent. The corresponding equation is:

$$q_t = K_i t^{\frac{1}{2}} + C \qquad \text{(Eq. III. 6)}$$

Where:

K_i: intraparticle diffusion rate constant [mg/g·min],

C: a constant related to the boundary layer thickness.

If the plot of qt versus $t^{1/2}$ is linear and passes through the origin, it indicates that intraparticle diffusion is the rate-limiting step. However, if the curve exhibits multiple linear phases, this suggests that other steps, such as external diffusion or chemical interaction, are influencing the adsorption process.

Analyzing these three models will help identify the primary kinetic mechanism governing the adsorption of hydrocarbons onto MCM-41 and Al-MCM-41 and allow for the optimization of industrial wastewater treatment conditions.

III.3. CHARACTERISTICS OF ADSORBENTS

The performance of an adsorbent material is strongly influenced by its physicochemical properties and its ability to interact with adsorbate species. Adsorbent materials are selected based on several essential criteria such as their texture, the chemical composition of their surface, and their thermal stability. These characteristics directly affect adsorption capacity, selectivity, and the reversibility of the process, which are crucial to ensuring the sustainability of the treatment system.

III.3.1. PROPERTIES OF ADSORBENT MATERIALS

The efficiency of adsorbent materials is influenced by their properties, particularly in the context of industrial wastewater treatment. Among the most significant characteristics are:

III.3.1.1. High Specific Surface Area

The specific surface area of a material, usually evaluated by the BET method (Brunauer, Emmett, and Teller), is a key factor for assessing its ability to adsorb molecules. An adsorbent with a high specific surface area offers a wide range of adsorption sites, thereby maximizing the pollutant capture capacity. Mesoporous materials, considered as promising adsorbents, can reach specific surface areas exceeding 1000 m^2/g [17].

III.3.1.2. Pore Volume and Pore Size Distribution

A material's ability to adsorb molecules of various sizes is influenced by its pore volume and the distribution of pore sizes. Mesoporous materials have intermediate-sized pores, typically ranging from 2 to 50 nm in diameter, which makes them particularly effective for hydrocarbon adsorption. Moreover, a well-balanced pore size distribution facilitates the diffusion of molecules throughout the porous network, enhancing optimal adsorption performance [18].

III.3.1.3. Chemical Nature of the Surface

The interaction between an adsorbent material and adsorbate species is influenced by the chemical state of its surface. The presence of silanol groups (Si–OH) on the surface of mesoporous materials enables the formation of hydrogen bonds with the adsorbed molecules, particularly in the case of hydrocarbons. In the structure of mesoporous materials, the incorporation of elements such as aluminum leads to the formation of Brønsted and Lewis

acid sites, thereby enhancing the material's ability to interact with polar molecules and promoting chemisorption [1].

III.3.1.4. Thermal and Mechanical Stability

A high-quality adsorbent must also exhibit exceptional thermal and mechanical stability in order to withstand demanding industrial conditions, such as high temperatures and pressures. Ordered mesoporous silicas possess excellent thermal resistance, making them well-suited for regeneration methods involving heating or washing [19].

III.3.2. TYPES OF ADSORBENT MATERIALS

Various categories of adsorbent materials exist, each with its own specific characteristics and applications. The main materials used in industrial adsorption processes include:

III.3.2.1. Activated Carbon

Activated carbon is one of the most widely used adsorbent materials due to its large specific surface area and its ability to adsorb a wide range of organic and inorganic compounds. It is mainly used for the adsorption of organic pollutants, such as hydrocarbons, in industrial wastewater treatment [20].

III.3.2.2. Mesoporous Silicas

Mesoporous silicas, such as MCM-41, are characterized by their high specific surface area and well-defined porous structures. They offer an alternative to activated carbon in applications requiring materials with controlled porosity and modifiable surface chemistry [21].

III.3.2.3. Zeolites

Zeolites, which belong to the tectosilicate group, are used in various fields such as adsorption and catalysis. Their robust crystalline structure and diverse chemical composition allow them to be highly selective toward specific molecules. However, their small pore size (< 2 nm) limits their ability to adsorb larger molecules, such as heavy hydrocarbons [22].

III.3.2.4. Functionalized Materials

Functionalized adsorbents are materials whose surfaces have been modified to incorporate specific functional groups that can interact more strongly with target pollutants. For example,

the incorporation of organic molecules into mesoporous materials enhances the interaction between hydrocarbons and the adsorbent surface, thereby increasing the retention capacity for the targeted species [23].

III.3.3. STUDIED MESOPOROUS MATERIALS

The use of mesoporous materials, particularly mesoporous silicas from the M41S family, offers promising prospects for the adsorption of hydrocarbons and organic pollutants in industrial wastewater. The two materials investigated in this study, MCM-41 and Al-MCM-41, are distinguished by their ordered hexagonal structure and large specific surface areas [1].

III.3.3.1. MCM-41

MCM-41 is a mesoporous silica-based solid composed of a hexagonal array of cylindrical pores and a highly specific surface area. The silanol groups (Si–OH) present on the surface of this material enable effective capture of certain organic molecules via physisorption, through hydrogen bonding interactions with pollutants. MCM-41 also exhibits high thermal stability, making it an ideal choice for regeneration cycles [24,25].

III.3.3.2. Al-MCM-41

Al-MCM-41 is a modified version of MCM-41 in which a portion of the silicon atoms has been replaced with aluminum, thereby creating Brønsted and Lewis acid sites. These acid sites enhance interaction with polar hydrocarbons, resulting in better performance for hydrocarbon adsorption compared to pure silica [26].
They increase the material's capacity to capture pollutants through chemisorption.

III.3.3.3. Grafting of MDEA

The performance of mesoporous materials can be further enhanced through chemical modifications of the surface of both materials under study. In this context, functionalization is carried out by grafting methyl diethanolamine (MDEA) onto the surface of MCM-41 and Al-MCM-41. The introduction of amine and hydroxyl functional groups through MDEA grafting results in increased polarity. Furthermore, the methyl group enhances chemical interactions with hydrocarbons by increasing the adsorption capacity, particularly in industrial environments where pollutants are present at low concentrations.

III.4. INTERACTIONS BETWEEN ADSORBENT AND POLLUTANT

The efficiency of an adsorption process relies on the interactions between the adsorbent and the pollutant. These interactions are primarily influenced by the physicochemical properties of the materials used as well as the characteristics of the adsorbate molecules [27]. This section examines the interactions between the mesoporous adsorbents MCM-41 and Al-MCM-41 and the hydrocarbons present in industrial wastewater. The nature of the adsorbent surfaces and the physicochemical parameters of the medium, such as pH, temperature, and pollutant concentration, impact these interactions.

III.4.1. INTERACTIONS BETWEEN ADSORBENTS AND HYDROCARBONS

Two main adsorption mechanisms are used to interpret surface interactions between mesoporous adsorbent materials and hydrocarbons: physisorption and chemisorption.

III.4.1.1. Physisorption

Physisorption occurs through weak forces such as van der Waals interactions and hydrogen bonding. Mesoporous materials like MCM-41 are covered with silanol groups (Si–OH), which can interact with hydrocarbon molecules via these forces. The pores of these materials trap nonpolar hydrocarbon molecules through these weak interactions without any chemical alteration of either the adsorbent or the adsorbate [28].

Regarding MCM-41, its fully siliceous surface facilitates the capture of light hydrocarbons and nonpolar compounds via physisorption [1]. When the material is functionalized with molecules such as MDEA, amine and hydroxyl groups are introduced onto its surface, enabling interactions not only with nonpolar hydrocarbons but also with polar compounds through physical interactions (van der Waals and hydrogen bonding).

III.4.1.2. Chemisorption

In the case of Al-MCM-41, the presence of aluminum in the structure leads to the formation of Brønsted and Lewis acid sites. Chemical interactions between the polar groups of certain hydrocarbons and the adsorbent surface are enhanced by these acid sites. Chemisorption occurs when polar hydrocarbon molecules interact with the acid sites of the adsorbent, resulting in the formation of covalent bonds or ionic interactions [29].

Polar hydrocarbons, such as those containing functional groups with oxygen atoms, are highly responsive to the Brønsted acid sites present on Al-MCM-41. Furthermore, the presence of

MDEA on the surface of Al-MCM-41 enhances these interactions by establishing hydrogen bonds with the amine and hydroxyl groups of MDEA, thereby increasing selectivity for polar hydrocarbons.

III.4.2. INFLUENCE OF PHYSICO-CHEMICAL PARAMETERS

The performance of an adsorbent material strongly depends on the physico-chemical characteristics of its environment. This thesis work mainly examines four key factors: adsorbent amount, agitation time, temperature, and pH of the medium.

III.4.2.1. Adsorbent mass

The adsorption capacity is directly influenced by the quantity of adsorbent used. Increasing the adsorbent mass enhances the number of available adsorption sites, thus improving pollutant capture. However, this quantity must be optimized to avoid excess adsorbent, which will not significantly improve adsorption efficiency once saturation is reached [30].

III.4.2.2. Agitation time

The adsorption kinetics is influenced by the agitation or contact time. Extending the agitation time allows adsorbate molecules to reach adsorption sites within the pores, increasing the amount of adsorbed species. Nevertheless, it is also necessary to determine the optimal time to reach adsorption equilibrium [31].

III.4.2.3. Temperature

Temperature affects adsorption processes. Increasing temperature can reduce adsorption efficiency by weakening van der Waals forces involved in physisorption. Conversely, in chemisorption, higher temperatures may promote active chemical exchanges. Therefore, temperature should be optimized according to the dominant type of adsorption [32].

III.4.2.4. pH

The pH of the environment impacts both the adsorbent surface and the adsorbate molecules. Interactions with pollutants can be influenced by pH, which affects the charge of functional groups present on the adsorbent surface. For example, during the grafting process with MDEA, a low pH favors the deprotonation of amine groups, enhancing interactions with hydrocarbons [21].

Moreover, the chemical nature of the adsorbent surface and the physicochemical conditions of the medium greatly influence interactions between mesoporous materials MCM-41, Al-MCM-41, and hydrocarbons. While MCM-41 primarily facilitates physisorption through weak interactions, Al-MCM-41 promotes stronger chemical adsorption due to its acid sites. By optimizing temperature, pH, and pollutant concentration conditions, adsorption can be effectively enhanced for versatile industrial systems.

III.5. CONCLUSION

In Chapter III, a thorough analysis of the mechanisms and factors influencing the adsorption process in the treatment of industrial wastewater was presented. The relationships between mesoporous adsorbent materials, such as MCM-41 and Al-MCM-41, and hydrocarbons were studied, highlighting the respective roles of physisorption and chemisorption. The chemical nature of the surface, the functionalization of materials with molecules such as MDEA, as well as the structural characteristics of the materials, were demonstrated to play a crucial role in the overall adsorption efficiency.

Moreover, physicochemical parameters such as adsorbent amount, agitation time, temperature, and pH were shown to be key factors for improving adsorption performance. These parameters not only influence the adsorption capacity of the materials but also affect the nature and strength of interactions with pollutants. Therefore, optimizing these parameters is essential to maximize the effectiveness of the process.

Furthermore, the use of appropriate mesoporous materials, combined with optimized adsorption conditions, enables the design of efficient solutions for the treatment of industrial wastewater contaminated especially by hydrocarbons. The results obtained in this chapter demonstrate that the studied materials, whether chemically modified or not, have significant potential for pollutant adsorption in complex industrial environments. These findings will serve as the foundation for the experiments and discussions presented in the following chapters.

Bibliographic references

[1] M. Maretto, R. Vignola, C.D. Williams, R. Bagatin, A. Latini, M.P. Papini, Adsorption of hydrocarbons from industrial wastewater onto a silica mesoporous material: Structural and thermal study, Microporous and Mesoporous Materials 203 (2015) 139–150.

[2] O. Ajumobi, B. Wang, A. Farinmade, J. He, J.A. Valla, V.T. John, Design of Nanostraws in Amine-Functionalized MCM-41 for Improved Adsorption Capacity in Carbon Capture, Design of Nanostraws in Amine-Functionalized MCM-41 for Improved Adsorption Capacity in Carbon Capture, Energy & Fuels 37 (2023) 12079–12088.

[3] C. Oleyar, J. Talbot, Reversible adsorption on a random site surface, Physica A: Statistical Mechanics and its Applications 376 (2007) 27–37.

[4] M. Atif, H.Z. Haider, R. Bongiovanni, M. Fayyaz, T. Razzaq, S. Gul, Physisorption and chemisorption trends in surface modification of carbon black, Surfaces and Interfaces 31 (2022) 102080.

[5] M. Thommes, K. Kaneko, A.V. Neimark, J.P. Olivier, F. Rodriguez-Reinoso, J. Rouquerol, K.S.W. Sing, Physisorption of gases, with special reference to the evaluation of surface area and pore size distribution (IUPAC Technical Report), Pure and Applied Chemistry 87 (2015) 1–19.

[6] X. Tian, Y. Song, Z. Shen, Y. Zhou, K. Wang, X. Jin, Z. Han, T. Liu, A comprehensive review on toxic petrochemical wastewater pretreatment and advanced treatment, Journal of Cleaner Production 245 (2020) 118692.

[7] S. Satyam, S. Patra, Innovations and challenges in adsorption-based wastewater remediation: A comprehensive review, Heliyon 10 (2024) e29573.

[8] V.M.S. Macedo, E.L. Gomes, J.C. Moreno-Piraján, L. Giraldo, L.P. Tovar, S.I.P.M.N. Alves, L.A.M. Ruotolo, R. Fernandez-Felisbino, Insights on the Synthesis of Al-MCM-41 with Optimized Si/Al Ratio for High-Performance Antibiotic Adsorption, ACS Omega 8 (2023) 48181–48190.

[9] L. Mohammadi, A. Rahdar, E. Bazrafshan, H. Dahmardeh, M.A.B.H. Susan, G.Z. Kyzas, Petroleum Hydrocarbon Removal from Wastewaters: A Review, Processes 8 (2020) 447.

[10] N. Kumar, A. Pandey, Rosy, Y.C. Sharma, A review on sustainable mesoporous activated carbon as adsorbent for efficient removal of hazardous dyes from industrial wastewater, Journal of Water Process Engineering 54 (2023) 104054.

[11] N. Chouat, A. Maziz, B. Bensafi, F. Djafri, Hierarchized ZSM-5 Zeolite Synthesis using N-Methyldiethanolamine as a Novel Desilicate Agent: Impact on Methanol Adsorption and Resistance

Improvement to Coke Poisoning, Journal of Inorganic and Organometallic Polymers and Materials (2024).

[12] O.P. Murphy, M. Vashishtha, P. Palanisamy, K.V. Kumar, A Review on the Adsorption Isotherms and Design Calculations for the Optimization of Adsorbent Mass and Contact Time, ACS Omega 8 (2023) 17407–17430.

[13] B. Bensafi, N. Chouat, F. Djafri, High performance of carbon dioxide adsorption of mesoporous mordenite synthesized in the presence of *N,N*-dimethylaniline, Research on Chemical Intermediates 43 (2017) 7443–7456.

[14] N. Ayawei, A.N. Ebelegi, D. Wankasi, Modelling and Interpretation of Adsorption Isotherms, Journal of Chemistry (2017) 3039817.

[15] A.A. Inyinbor, F.A. Adekola, G.A. Olatunji, Kinetics, isotherms and thermodynamic modeling of liquid phase adsorption of Rhodamine B dye onto Raphia hookerie fruit epicarp, Water Resources and Industry 15 (2016) 14–27.

[16] C.M.A.C. Alves, J.F. Alves, L.L. Bezerra, L.P. da Silva, N.K.V. Monteiro, R.C. Rabelo-Neto, R.S. Araújo, M.L.M. Oliveira, Adsorption of linear and cyclic pentasiloxanes onto MCM-41: Experimental and computational studies, Results in Surfaces and Interfaces 18 (2025) 100382.

[17] Y. Wang, Z. Chen, L. Hu, Determining the Geometric Surface Area of Mesoporous Materials, The Journal of Physical Chemistry C 127 (2023) 4799–4807.

[18] M. Eskandari-Ghadi, Y. Zhang, Effect of pore size distribution on sorption-induced deformation of porous materials: A theoretical study, International Journal of Solids and Structures 242 (2022) 111533.

[19] M.S. Akhtar, S. Ali, W. Zaman, Innovative Adsorbents for Pollutant Removal: Exploring the Latest Research and Applications, Molecules 29 (2024) 4317.

[20] W. Ahmad, T. Muhammad, I. Ahmad, M. Khan, S. Nazneen, Adsorption of hydrocarbon pollutants from wastewater using Cu- and Zn-loaded activated carbon derived from waste tires, Environmental Progress & Sustainable Energy 43 (2024) e14360.

[21] T.M. Albayati, K.R. Kalash, Polycyclic aromatic hydrocarbons adsorption from wastewater using different types of prepared mesoporous materials MCM-41in batch and fixed bed column, Process Safety and Environmental Protection 133 (2020) 124–4136.

[22] L.S. Migliorin, D.S.P. Franco, S. Knani, J. Georgin, L.A. Vieira, M.R. Monteiro, S.L. Jahn, G.L. Dotto, Application of mesoporous zeolite Socony Mobil-5 (ZSM-5) as an adsorbent material for the removal of naphthenic acid present in oil-produced water, Microporous and Mesoporous Materials 344 (2022) 112216.

[23] L. Song, T. Bu, L. Zhu, Y. Zhou, Y. Xiang, D. Xia, Synthesis of Organically–Inorganically Functionalized MCM-41 for Adsorptive Desulfurization of C4 Hydrocarbons, The Journal of Physical Chemistry C 118 (2014) 9468–9476.

[24] J. Stocki, M. Kuśmierz, W. Sofińska-Chmiel, M. Stankevič, M. Puchała, M.A. Kojdecki, R. Gąska, H. Grajek, Parametric Modelling of the Crystalline Microstructure of the MCM41-Type Mesoporous Silica Modified with Derivatives of Alkyls, Materials 17 (2024) 3065.

[25] G. Martínez-Edo, A. Balmori, I. Pontón, A.M. del Rio, D. Sánchez-García, Functionalized Ordered Mesoporous Silicas (MCM-41): Synthesis and Applications in Catalysis, Catalysts 8 (2018) 617.

[26] M. Selvaraj, A. Pandurangan, K.S. Seshadri, P.K. Sinha, V. Krishnasamy, K.B. Lal, Comparison of mesoporous Al-MCM-41 molecular sieves in the production of p-cymene for isopropylation of toluene, Journal of Molecular Catalysis A: Chemical 86 (2002) 173–186.

[27] F. Amalina, A.S. Abd Razak, Sa. Krishnan, A.W. Zularisam, M. Nasrullah, The effects of chemical modification on adsorbent performance on water and wastewater treatment - A review, Bioresource Technology Reports 20 (2022) 101259.

[28] M.R. Mello, D. Phanon, G.Q. Silveira, P.L. Llewellyn, C.M. Ronconi, Amine-modified MCM-41 mesoporous silica for carbon dioxide capture, Microporous and Mesoporous Materials 143 (2011) 174–179.

[29] R. Locus, D. Verboekend, R. Zhong, K. Houthoofd, T. Jaumann, S. Oswald, L. Giebeler, G. Baron, B.F. Sels, Enhanced Acidity and Accessibility in Al-MCM-41 through Aluminum Activation, Chemistry of Materials 28 (2016) 7731–7743.

[30] S. Satyam, S. Patra, Innovations and challenges in adsorption-based wastewater remediation: A comprehensive review, Heliyon 10 (2024) e29573.

[31] O.P. Murphy, M. Vashishtha, P. Palanisamy, K.V. Kumar, A Review on the Adsorption Isotherms and Design Calculations for the Optimization of Adsorbent Mass and Contact Time, ACS Omega 8 (2023) 17407–17430.

[32] K.S.N. Kamarudin, N. Alias, Adsorption performance of MCM-41 impregnated with amine for CO_2 removal, Fuel Processing Technology 106 (2013) 332–337.

CHAPTER IV
Experimental Procedures

Table of Contents

CHAPTER IV. Experimental Procedures

List of tables

In this chapter, we present the different methodological steps and approaches used to carry out this investigation. The process begins with the synthesis and preparation of mesoporous adsorbent materials, including functionalization modifications to enhance their adsorption efficiency. The choice was made to work with MCM-41, Al-MCM-41, and their grafted versions due to their exceptional porosity properties, high specific surface area, and chemical interaction capabilities.

Analytical techniques are employed to characterize the physicochemical properties of all samples. Performing these analysis ensures that the materials meet the necessary criteria for reliable adsorption testing. Subsequently, the adsorption analysis is deepened by examining the factors influencing the process, the experimental techniques used, and by interpreting the results based on theoretical models. The objective of this approach is to develop a thorough understanding of the interaction mechanisms between adsorbents and hydrocarbons present in industrial wastewater.

IV.1. MATERIALS SYNTHESIS

The fabrication of mesoporous materials such as MCM-41 and Al-MCM-41 is a crucial step for their use as adsorbents. These materials are synthesized using the sol-gel method coupled with a structure-directing agent, which allows control over pore size and chemical composition. In this study, specific adjustments, such as the incorporation of aluminum and the addition of organic molecules, aim to improve their adsorption capacities for various hydrocarbons. This section details the synthesis procedures, experimental conditions, and modifications applied to obtain materials with optimal characteristics that meet the requirements for adsorption tests.

IV.1.1. MATERIALS AND PRODUCTS

The fabrication of mesoporous materials MCM-41 and Al-MCM-41 involves silicate and aluminate precursors in the presence of a structure-directing agent (CTABr) to create a well-defined porous structure. A hydrothermal process followed by careful calcination is used to provide the materials with the required textural and crystallographic properties for applications, notably in adsorption. Table IV.1 lists the reactive substances and equipment used in this experimental stage.

Table IV.1. Reagents and Equipment Used for the Synthesis of M41S Materials

Reagents/Equipment	Quantity		Function
	MCM-41	**Al-MCM-41**	
CTABr (cetyltrimethylammonium bromide)	2,9156 g	2,9156 g	Structure-directing agent (template)
NaOH	0,666 g	0,666 g	Alkaline agent
TEOS (tetraethyl orthosilicate)	13,88 g	13,88 g	Silica source
$NaAlO_2$ (sodium aluminate)	-	0,137 g	Aluminum source (for Al-MCM-41)
Ethanol (EtOH)	4,6 g	4,6 g	Solvent
Deionized water	120 g	120 g	Solvent
Autoclave	-	-	Hydrothermal crystallization
Oven (150 °C and 80 °C)	-	-	Heating and drying
Nabertherm furnace (550 °C)	-	-	Calcination

The objective of grafting MDEA onto the mesoporous materials MCM-41 and Al-MCM-41 is to enhance their adsorption capacity through functionalization. The use of an organic solvent (toluene) and a mild catalyst (NH_4Cl) is necessary to promote the formation of covalent bonds between MDEA and the surface of the material. The reagents and equipment required for this operation are listed in Table IV.2.

Table IV.2. Reagents and Equipment Required for the Grafting Operation of MDEA

Reagents/Equipment	Quantity	Function
MCM-41 / Al-MCM-41	5 g	Base material
MDEA (methyl diethanolamine)	1.5 g (0.015 mol)	Grafting molecule
Anhydrous toluene	300 mL	Reaction solvent
NH_4Cl (ammonium chloride)	0.5 g	Catalyst and buffer
Anhydrous ethanol	50 mL	Final washing
Three-neck flask	–	Grafting reactor
Reflux condenser	–	Vapor condensation
Heating mantle (80 °C)	–	Solution heating
Magnetic stir bar	–	Solution stirring
Büchner filter	–	Material recovery
Vacuum pump	–	Filtration acceleration
Oven (80–120 °C)	–	Drying

IV.1.2. SYNTHESIS OF M41S MATERIALS

The synthesis protocol for MCM-41 and Al-MCM-41 materials was carried out as follows [1]:

1. Preparation of solutions:

Solution 1: Dissolve 2.9156 g of CTABr and 0.137 g of sodium aluminate (aluminum source for Al-MCM-41) in 100 g of distilled water, then add 4.6 g of ethanol. Stir vigorously at 35 °C for 30 minutes until the solution is homogeneous.

Solution 2: Dissolve 0.666 g of NaOH in 20 g of distilled water. Stir continuously for 10 minutes until a clear alkaline solution is obtained.

Solution 3: Prepare 13.88 g of TEOS (silica source) to be added later.

2. Procedure:

Gradually add Solution 2 into Solution 1 under continuous stirring. Maintain agitation for an additional 10 minutes to ensure homogenization. Then, add Solution 3 dropwise into the mixture while stirring. Continue stirring the resulting mixture for 3 hours at 35 °C to promote the formation of the reactive gel.

Transfer the final mixture into a stainless-steel autoclave. Perform hydrothermal treatment at 150 °C for 24 hours under autogenously pressure. This process enables the formation of ordered mesoporous structures typical of MCM-41 or Al-MCM-41.

The molar compositions of the two mesoporous materials are as follows:

MCM-41: SiO_2 - 0,12 CTABr – 0,25 NaOH - 1,5 EtOH - 100 H_2O

Al-MCM-41: SiO_2 - 0,025 Al_2O_3 - 0,12 CTABr – 0,25 NaOH - 1,5 EtOH - 100 H_2O

After crystallization, filter the resulting solid and wash several times with deionized water to remove residual reagents. Dry the solid at 80 °C overnight (approximately 12 hours).

To develop porosity, the dried materials are calcined at 550 °C for 6 hours under a static atmosphere to remove all traces of the organic structure-directing agent.

IV.1.3. GRAFTING OF MDEA ONTO MCM-41 AND Al-MCM-41

The grafting of the organic molecule was developed in our laboratory. Begin by placing 5 g of MCM-41 or Al-MCM-41 in an oven at 120 °C for 2 hours to eliminate any physiosorbed moisture on the surfaces of the two materials. This thermal activation step helps remove water molecules from silanol (Si–OH) or hydroxyl (Al–OH) groups, preparing the material for functionalization.

Simultaneously, dissolve 1.5 g of MDEA (0.015 mol) in 300 mL of anhydrous toluene to achieve a concentration of 0.05 M. Then add 0.5 g of NH_4Cl, which acts as a catalyst for the condensation reaction and as a buffer to mitigate the potential desilication effect caused by MDEA.

Add the 5 g of activated MCM-41 or Al-MCM-41 to the grafting solution. Using a reflux condenser and a heating mantle, insert a magnetic stir bar into the flask and begin stirring at a moderate speed (approximately 400 rpm). Heat the solution to 80 °C (a moderate reflux temperature to prevent desilication) and maintain under reflux for 24 hours.

During this time, MDEA reacts with hydroxyl groups (Si–OH or Al–OH) on the surface of the materials via a condensation reaction, forming covalent Si–O–MDEA or Al–O–MDEA bonds, as illustrated in the following chemical reactions:

Si-OH + MDEA → Si-O-MDEA + H_2O

Al-OH + MDEA → Al-O-MDEA + H_2O

After completing the reaction, allow the suspension to cool to room temperature. The grafted solid should then be vacuum filtered using a Büchner funnel to separate the mesoporous grafted material from the reaction solution. To remove excess MDEA and unreacted by-products, the grafted solid must be washed several times with anhydrous toluene (approximately 30–50 mL), followed by a final rinse with 50 mL of anhydrous ethanol to eliminate any remaining impurities.

The grafted adsorbent is then transferred to an oven set at 80 °C and dried overnight to completely remove residual solvents and stabilize the covalent bonds formed between MDEA and the adsorbent.

IV.2. CHARACTERIZATION TECHNIQUES

The analysis of the structural, chemical, textural, and morphological properties of the materials is a crucial step in evaluating their adsorption efficiency. In this thesis work, a set of analytical techniques was employed to gain a comprehensive understanding of the MCM-41 and Al-MCM-41 materials, as well as their functionalized counterparts.

The crystalline structure of the samples was confirmed by X-ray diffraction (XRD), while X-ray fluorescence (XRF) provided information on their elemental composition. Specific functional groups were identified using Fourier-transform infrared spectroscopy (FTIR), and their thermal stability was assessed through thermogravimetric analysis (TGA/DSC).

Textural properties were evaluated using BET surface area analysis, and scanning electron microscopy (SEM) was employed to obtain insights into the morphology and particle distribution. These characterization methods provide a solid foundation for the study of adsorption performance.

IV.2.1. X-RAY DIFFRACTION (XRD)

The crystalline structure of the materials was analyzed using X-ray diffraction (XRD) with a Bruker D8 ADVANCE diffractometer equipped with a CuKα radiation source (λ = 1.5406 Å). The mesoporous samples were scanned over a 2θ angular range from 1° to 10°, with a step size of 0.02° and a counting time of 1 second per step. This technique enables the assessment

of the mesostructured organization of the materials by identifying characteristic diffraction peaks associated with the hexagonal pore arrangement. The obtained results allowed the determination of structural parameters such as interplanar spacing and pore dimensions, which are essential for verifying the quality of the synthesis and detecting changes induced by functionalization [2].

IV.2.2. X-RAY FLUORESCENCE (XRF)

The chemical composition of the materials was examined using X-ray fluorescence (XRF) with the S8 Tiger spectrometer (Bruker GmbH, Karlsruhe, Germany). Pressed powder samples were exposed to an X-ray beam to identify the elements present and quantify their concentrations. Analyses were conducted at an operating voltage of 50 kV and a current of 1 mA, using a Si(Li) detector to enhance sensitivity. This method enabled the determination of the elemental composition of the materials, verification of the Si/Al ratio in Al-MCM-41 samples, and detection of potential impurities. Gathering this information is crucial for correlating chemical composition with the adsorption performance of the materials [3].

IV.2.3. FOURIER TRANSFORM INFRARED SPECTROSCOPY (FTIR)

The functional groups present in the materials were identified using FTIR spectroscopy with an Alpha-Bruker FTIR spectrophotometer equipped with an ATR (Attenuated Total Reflectance) accessory. Spectra were recorded over the range of 4000 to 500 cm^{-1}, with a resolution of 4 cm^{-1} and 32 scans per sample. This technique made it possible to detect characteristic vibrations of Si–O and Si–OH bonds, as well as those associated with grafted organic groups, such as those derived from MDEA. The FTIR results play a crucial role in assessing the chemical modifications introduced to the materials and in understanding potential interactions with target molecules during adsorption tests [4].

IV.2.4. THERMAL ANALYSES

Thermogravimetric analysis (TGA) and differential thermal analysis (DTA) were performed using a TA Micrometrics 2050 TGA analyzer. The samples were subjected to a temperature range of 25 to 800 °C at a heating rate of 10 °C/min under an oxygen atmosphere. TGA enabled the monitoring of mass losses due to the removal of adsorbed water, residual organic

compounds, or grafted groups, while DTA allowed the detection of thermal transitions associated with these characteristics. The results revealed the thermal stability of the materials and the critical temperatures for their modification, ensuring their compatibility with the experimental conditions of the adsorption tests [5].

IV.2.5. TEXTURAL ANALYSES

Understanding the correlation between the textural properties of materials and their adsorption capacity is essential. For this purpose, a BET analysis was conducted to measure specific surface area, pore volume, and pore size using a Micromeritics ASAP 2020 porosimeter. The samples were degassed at 300 °C under vacuum for 12 hours to eliminate any traces of moisture or impurities. Nitrogen adsorption-desorption isotherms were recorded at -196 °C. The obtained data allowed for the determination of all key textural parameters [6].

IV.2.6. SCANNING ELECTRON MICROSCOPY (SEM)

The materials were analyzed using scanning electron microscopy with a JEOL JSM 6610 LA microscope. Prior to analysis, the samples were coated with a thin layer of gold to enhance their conductivity. Images were taken at an accelerating voltage of 5 kV, allowing for high-resolution observation of surface texture and particle distribution. This method enabled the identification of phenomena such as particle agglomeration and morphological changes caused by chemical modifications [6].

IV.3. ADSORPTION TESTS

Adsorption experiments are a crucial step in evaluating the capacity of mesoporous materials to remove hydrocarbons present in industrial wastewater. These tests assess the ability of the materials to adsorb various organic molecules found in the pollutant load, whether polar, such as methanol and/or ethylene glycol, or non-polar, such as heavy alkanes.

Experimental parameters—including the amount of adsorbent, solution pH, temperature, and contact time—were carefully adjusted to simulate real industrial environments. The resulting data were analyzed to deepen the understanding of the interaction mechanisms between hydrocarbons and the active surfaces of the adsorbents, taking into account their structural and physicochemical characteristics.

IV.3.1. SAMPLING PROCEDURE

A rigorous method was used to sample industrial wastewater containing hydrocarbons to ensure the representativeness and reliability of the results. Samples were collected after the screening treatment carried out using the CPI (Corrugated Plate Interceptor) process, which separates free oils and floating solids from the water. This preliminary step is essential to obtain a wastewater matrix primarily composed of residual hydrocarbons, which were used for the adsorption study.

To preserve sample integrity, brown glass bottles were used, as they protect volatile organic compounds and light-sensitive hydrocarbons while preventing chemical interactions with the storage material. Prior to final sampling, each bottle was rinsed three times with the sample to avoid cross-contamination.

Before analysis, the samples were transported and stored at 4 °C to minimize chemical or biological changes. This protocol ensures sample quality and provides reliable data to evaluate the adsorption performance of the materials.

IV.3.2. ADSORPTION TEST METHODOLOGY

The methodology used for the adsorption tests is based on well-defined steps to ensure reproducibility and accuracy of the results. It includes the preparation of the experimental setup, implementation of the experimental protocol, and analysis of the samples after adsorption to evaluate the materials' efficiency.

IV.3.2.1. Experimental Setup

The experimental setup was designed to ensure homogeneous conditions during the adsorption tests. It includes a magnetic stirrer to maintain constant agitation of the suspensions and a thermostatic cell to control the temperature. A glass beaker was used to hold the wastewater solution and the adsorbent.

IV.3.2.2. Experimental Protocol

To begin the tests, several experimental parameters were varied to optimize operating conditions, starting with the mass of the adsorbent. Each adsorption test followed the steps below:

- Homogenization of the wastewater solution, followed by transferring 20 mL of hydrocarbon-containing wastewater into a beaker;

- Addition of a known mass of adsorbent into the beaker;
- Adjustment of the parameters according to the experimental conditions studied (adsorbent mass, stirring time, working temperature, and pH of the medium);
- Agitation of the mixture for a predetermined period until adsorption equilibrium was reached;
- Vacuum filtration of the solutions to separate solid particles after the test.

IV.3.2.3. Analysis of Solutions after Adsorption

The wastewater samples were analyzed after adsorption using the HORIBA OCMA-310 hydrocarbon-in-water analyzer, a reliable instrument for accurately assessing the residual hydrocarbons present in aqueous solutions. This system employs solvent extraction, specifically using the renewable solvent S-316, which is specially formulated for effective and environmentally friendly hydrocarbon extraction.

After each adsorption test, the samples were treated by adding a specific amount of S-316 solvent to extract the remaining hydrocarbons from the water. The extracted solution was then introduced into the OCMA-310, where an infrared sensor performed the detection, ensuring precise quantification.

The performance of the mesoporous materials (MCM-41, Al-MCM-41, and their functionalized derivatives) was evaluated by measuring the residual hydrocarbon concentrations after adsorption. These included both polar molecules such as methanol, ethanol, and ethylene glycol, and non-polar hydrocarbons ranging from C6+ (hexane and above). The amount of hydrocarbons adsorbed was calculated using the following equation [7]:

$$Q_{ads} = \frac{(C_{ini} - C_{res}) \times V_{water}}{m_{ads}} \quad \text{(Eq. IV.1)}$$

Where:

C_{ini} : Initial hydrocarbon concentration [mg]

C_{res} : Residual hydrocarbon concentration after adsorption [mg]

V_{Water}: Volume of the stirred solution [L]

m_{ads}: Mass of the adsorbent used [g]

This approach enables accurate measurement of the adsorption efficiency of the tested mesoporous materials, taking into account the chemical composition of the hydrocarbons.

Bibliographic references

[1] B. Boukoussa, S. Zeghada, G.B. Ababsa, R. Hamacha, A. Derdour, A. Bengueddach, F. Mongin, Catalytic behavior of surfactant-containing-MCM-41 mesoporous materials for cycloaddition of 4-nitrophenyl azide, Applied Catalysis A: General 489 (2015) 131–139.

[2] D.E. Romero, M. Rigutto, E.J.M. Hensen, Influence of the size, order and topology of mesopores in bifunctional Pd-containing acidic SBA-15 and M41S catalysts for n-hexadecane hydrocracking, Fuel Processing Technology 232 (2022) 107259.

[3] M. Szeląg, M. Janek, R. Panek, J. Madej, J. Fronczyk, Modification of the MCM-41 mesoporous silica and its influence on the hydration and properties of a cement matrix, Construction and Building Materials 344 (2022) 128253.

[4] A. Szegedi, M. Popova, I. Goshev, S. Klébert, J. Mihály, Controlled drug release on amine functionalized spherical MCM-41, Journal of Solid State Chemistry 194 (2012) 257–263.

[5] J. Pires, Simultaneous Thermogravimetry-Differential Scanning Calorimetry (TG-DSC) in Nanoporous Materials: Examples of Data for Zeolites, Metal–Organic Frameworks (MOFs), Clay Based and Mesostructured Solids, Journal of Inorganic and Organometallic Polymers and Materials 34 (2024) 3346–3359.

[6] O. Ajumobi, B. Wang, A. Farinmade, J. He, J.A. Valla, V.T. John, Design of Nanostraws in Amine-Functionalized MCM-41 for Improved Adsorption Capacity in Carbon Capture, Energy & Fuels 37 (2023) 12079–12088.

[7] C.M.A.C. Alves, J.F. Alves, L.L. Bezerra, L.P. da Silva, N.K.V. Monteiro, R.C. Rabelo-Neto, R.S. Araújo, M.L.M. Oliveira, Adsorption of linear and cyclic pentasiloxanes onto MCM-41: Experimental and computational studies, Results in Surfaces and Interfaces 18 (2025) 100382.

CHAPTER V

Results And Discussion

Table of Contents

CHAPTER V. Results And Discussion

List of Figures

List of tables:

This chapter presents and analyzes the experimental results obtained in this study. It is structured in several sections, covering material characterization, hydrocarbon adsorption tests and model evaluation. First, however, we will present the synthesis data and characterization results for the mesoporous materials (MCM-41 and Al-MCM-41), in order to confirm their structure, chemical composition and textural and morphological properties. Next, the results of adsorption tests will be presented in graphical and tabular form, together with an analysis of the materials' performance in relation to their characteristics.

Finally, we will evaluate adsorption parameters by comparing them with theoretical models, notably the Langmuir, Freundlich and Temkin isotherms. These analyses will enable us to interpret the adsorption mechanisms involved and assess the effectiveness of the materials developed for hydrocarbon removal from industrial wastewater. All these results will be discussed in relation to the hypotheses established in CHAPTER III and compared with literature data to provide a thorough understanding of the behavior of the materials studied.

V.1. CHARACTERIZATION of MATERIALS

Characterization of synthesized materials is an essential step in assessing their structure, chemical composition and textural properties. It allows us to verify the success of the synthesis and to establish correlations between the properties of the samples developed and their adsorption performance. Various analyses were carried out to identify the porous structure, the distribution of elements, and the molecular interactions present within the materials. The results obtained provide valuable information on the organization of the porous network and the thermal stability of the samples, aspects which are crucial to their effectiveness in the adsorption process.

In addition, four samples were synthesized and characterized: purely silicic MCM-41 (B1), aluminum-containing Al-MCM-41 with Si/Al ratio = 40 (B2), MCM-41 grafted with methyl diethanolamine (MDEA-MCM-41, B3) and Al-MCM-41 functionalized with MDEA (MDEA-Al-MCM-41, B4). These samples were named B1, B2, B3 and B4 respectively, to facilitate their identification and assess the impact of aluminum incorporation and organic grafting on their structural and textural properties.

V.1.1. X-RAY DIFFRACTION

The X-ray diffraction (XRD) patterns of the four synthesized samples are shown in Figure V.1.

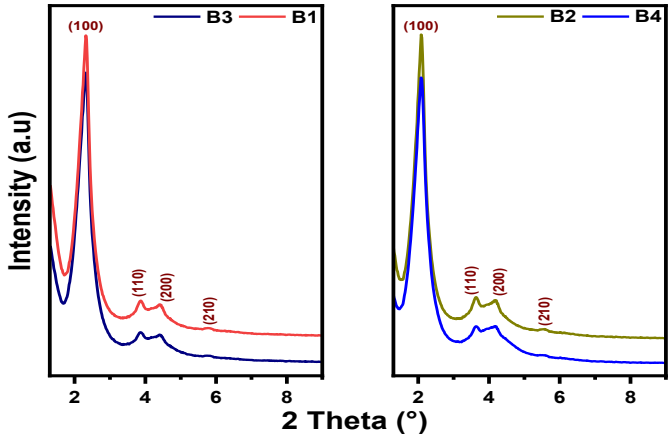

Figure V. 1. *X-ray diffractograms of samples B1, B2, B3, and B4.*

The X-ray diffraction (XRD) patterns of the four samples (B1, B2, B3, and B4) reveal characteristic peaks corresponding to the well-ordered hexagonal structure typical of MCM-41-type materials, identified by the (100), (110), (200), and (210) reflections [1]. For the purely siliceous MCM-41 (B1), the peaks at 2.32°, 3.87°, 4.59°, and 5.82° indicate a stable mesoporous organization, whereas the incorporation of aluminum in Al-MCM-41 (B2) shifts these reflections slightly to 2.12°, 3.66°, 4.16°, and 5.56°, suggesting a unit cell expansion caused by the partial substitution of silicon with aluminum (Al). This incorporation of Al into the silica framework alters the interplanar spacing, which is consistent with the larger ionic radius of aluminum and the formation of acid sites within the structure [2].

The effect of MDEA grafting is also noticeable: in the case of grafted MCM-41 (B3), the peaks remain close to those of the ungrafted material (B1), with minor shifts of about 0.02° toward lower angles, indicating that the mesoporous structure is preserved despite the presence of organic molecules on the pore walls. However, a slight decrease in peak intensity can be observed, potentially attributable to partial pore filling by MDEA. For the grafted Al-MCM-41 (B4), the (100), (110), (200), and (210) reflections also remain visible, but with a shift of approximately 0.01° toward lower angles and a change in intensity compared to the ungrafted sample (B2), indicating that MDEA grafting did not destroy the mesoporous organization [3]. However, the combination of aluminum incorporation and organic grafting may amplify structural disturbances, resulting in a slight reduction in pore ordering.

Overall, these results confirm the successful synthesis of mesoporous materials and show that aluminum induces a shift toward lower 2θ values, while MDEA grafting primarily affects the intensity and definition of the diffraction peaks, all while preserving the fundamental hexagonal mesoporous structure.

The unit cell parameter a_0 was calculated using the following equation [2]:

$$a_0 = \frac{2d_{100}}{\sqrt{3}} \quad \text{(Eq. V.1)}$$

Accordingly, the interplanar spacing values d_{100} were determined based on Bragg's law:

$$d_{100} = \frac{n\lambda}{2\sin\theta} \quad \text{(Eq. V.2)}$$

With λ = 1,5406 Å. The results obtained for d_{100} and the unit cell parameter a_0 (Table V.1) confirm the hexagonal arrangement of the materials and their classification within the p6mm space group.

Table V. 1. Lattice parameters of samples B1, B2, B3, and B4.

Material	**2θ (°)**	**d_{100} (Å)**	**a_0 (Å)**
B1	2,32	38,05	43,94
B2	2,12	41,64	48,07
B3	2,30	38,38	44,3
B4	2,11	41,84	48,3

The analysis of the d_{100} values shows that the incorporation of aluminum causes a slight increase in the interplanar spacing (from 38.05 Å for MCM-41 to 41.64 Å for Al-MCM-41). Similarly, modification with MDEA moderately affects these parameters, with values of 38.38 Å for MDEA-MCM-41 and 41.84 Å for MDEA-Al-MCM-41 (compared to 41.64 Å for Al-MCM-41). These variations indicate a structural modification influenced by the chemical nature of the materials.

V.1.2. X-RAY FLUORESCENCE

The elemental chemical composition analysis of the four samples B1, B2, B3, and B4, carried out by X-ray fluorescence spectroscopy, is presented in Table V.2.

Table V.2. Elementary composition of samples B1, B2, B3, and B4 determined by XRF spectroscopy.

Material	**Si (%)**	**O (%)**	**Al (%)**	**C (%)**	**N (%)**	**H (%)**	**RSA***
B1	50,24	48,75	-	-	-	1,01	-
B2	48,36	48,12	1,07	-	-	1,45	45,36
B3	46,18	45,66	0	4,21	1,58	2,37	-
B4	45,02	45,05	1,03	4,78	1,73	2,39	43,69

* : Rapport Si/Al

Elemental chemical analysis by XRF of the four samples, namely B1, B2, B3, and B4, revealed significant variations in chemical composition, illustrating the combined effects of aluminum incorporation and organic grafting. Sample B1 is characterized by a composition predominantly composed of silicon (Si) and oxygen (O), with an infinite Si/Al ratio, confirming the complete absence of aluminum and the exclusive presence of silica.

The introduction of aluminum in B2 led to a reduction in the silicon percentage (from 50.24% to 48.36%) and the appearance of an aluminum mass fraction of 1.07%, perfectly matching the targeted molar Si/Al ratio of 40. This partial substitution of Si by Al within the mesoporous network induces a notable change in the material's acid-base and hydrophilic properties, directly influencing its adsorption behavior [4].

Grafting MDEA onto MCM-41 (B3) results in a significant increase in carbon and nitrogen contents rises respectively from 0 to 4.21% and 0 to 1.58%, confirming the anchoring of methyl- and diethanolamine groups on the porous surface. This grafting is also evidenced by an increase in hydrogen content, reaching 2.37%, due to the presence of hydroxyl (O-H), methyl (CH3), and methylene (-CH2-) groups from MDEA [1].

When MDEA is grafted onto Al-MCM-41 (B4), similar trends are observed, with increased carbon (4.78%) and nitrogen (1.73%) levels, but also a slight desilication of the material. This silicon loss, confirmed by the decrease in the measured Si/Al ratio after grafting (from 45.36 to 43.69), is attributed to the complexing effect of MDEA, which, under locally basic conditions, promotes partial extraction of Si from the structure [5].

V.1.3. TEXTURAL ANALYSIS

Figure V.2 presents the nitrogen adsorption-desorption isotherms at -196 °C, along with the mesopore size distribution curves obtained by the BJH method for the four samples B1, B2, B3, and B4.

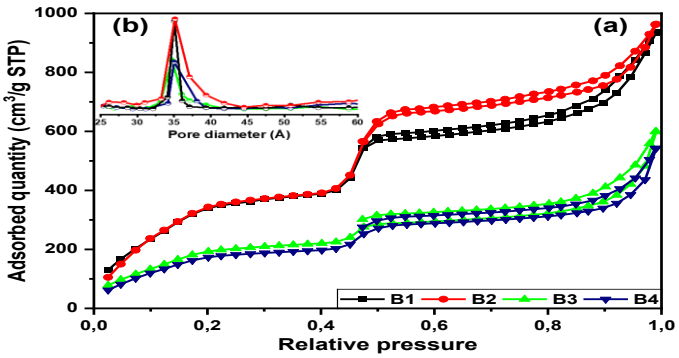

Figure V. 2. (a) Nitrogen adsorption-desorption isotherms at -196 °C; (b) Mesopore distribution obtained by the BJH method for the four samples B1, B2, B3, and B4.

The BET analysis of the studied materials reveals significant trends related to the mesoporous structure and the impact of grafting on textural properties. All nitrogen adsorption-desorption isotherms, shown by the experimental curves, exhibit type IV (a) behavior according to the IUPAC classification, characterized by a saturation plateau of variable length at relative pressures above 0.42, accompanied by hysteresis. This type of isotherm is typical for mesoporous adsorbents where capillary condensation occurs [6].

These isotherms display H1-type hysteresis loops, with parallel adsorption and desorption branches, observed for adsorbents with a very narrow mesopore size distribution. This feature suggests well-defined pores and pronounced capillarity. However, the BJH analysis of the desorption curves provides the mesopore size distribution and confirms the trends observed by BET. Table V.3 summarizes the main textural properties of our materials [6].

Table V. 3. Main textural properties of samples B1, B2, B3, and B4.

Material	Si/Al[a]	d_{100} (Å)	a_0 (Å)[b]	S_{BET} (m²/g)	D_p (Å)[c]	h (Å)[d]	V_p (cm³/g)
B1	-	38,05	43,94	1392	34,9	9,04	1,067
B2	45,36	41,64	48,07	1411	35,1	12,97	1,093
B3	-	38,38	44,3	789	34,7	9,6	0,602
B4	43,69	41,84	48,3	707	35	13,3	0,578

a : par analyse FRX
b : paramètre de maille = $2d_{100}/\sqrt{3}$
c : diamètre de pore déterminer par la méthode BJH
d : épaisseur de la paroi = a_0 - D_p

Samples B1 and B2 exhibit a uniform distribution of mesopores with diameters centered around 34.9 Å and 35.1 Å, respectively, consistent with their H1-type hysteresis loops. In contrast, samples B3 and B4 show a partial broadening of the mesopore distribution, suggesting a modification of the internal connectivity and partial blockage of channels due to grafting.

Moreover, material B1 displays a high specific surface area of 1392 m^2/g, indicating a highly porous structure with a relatively thin wall thickness (9.04 Å). Its pore volume of 1.067 cm^3/g reflects well-developed porosity, in agreement with its structural organization. Material B2 exhibits similar characteristics, with a slightly higher specific surface area (1411 m^2/g) and a pore volume of 1.093 cm^3/g, confirming the stability of the mesoporous network. The increase in the unit cell parameter a_0 (48.07 Å for B2 compared to 43.94 Å for B1) suggests an expansion of the framework due to aluminum incorporation into the material composition [2].

Conversely, materials B3 and B4 show a significant reduction in specific surface area, reaching 789 m^2/g and 707 m^2/g, respectively. This decrease is accompanied by a reduction in pore volume (0.602 cm^3/g for B3 and 0.578 cm^3/g for B4), indicating a structural modification affecting pore connectivity. This textural evolution suggests that grafting has induced an alteration of the pore architecture, likely due to stronger interactions between the grafted groups and the material surface [1].

The BJH analysis indicates that the average mesopore size remains overall unchanged after grafting (approximately 35 Å), but the mesopore distribution in B3 and B4 becomes slightly broader, suggesting a local modification of the pore network. This phenomenon may be attributed to slight desilication induced by MDEA [5], leading to a partial redistribution of pore sizes, as well as to the occupation of mesopores by grafted molecules, thus limiting accessibility to internal sites.

Furthermore, the wall thickness increases, notably for B4 (13.3 Å), reflecting a grafting effect that reduces accessible porosity due to partial mesopore blockage. This phenomenon is reinforced by the more pronounced decrease of S_BET and V_p for B4 compared to B3, suggesting that the incorporation of grafted species was more effective and led to a stronger reorganization of the pore network [7].

Furthermore, the BET and BJH analyses highlight the influence of grafting on the mesoporous architecture of the materials. While samples B1 and B2 retain a high porosity with well-defined mesopores, their more open structure promotes increased accessibility to

active sites. Conversely, B3 and B4 undergo a reduction in porosity, likely due to deposition within the pores that disrupts their connectivity. These textural modifications are consistent with the results obtained from XRD and XRF analyses.

V.1.4. FOURIER TRANSFORM INFRARED SPECTROSCOPY (FTIR)

The FTIR analysis of the four materials enables the identification of the functional groups present and the evaluation of chemical changes induced by the incorporation of aluminum or the post-synthesis grafting of MDEA. Figure V.3 shows the FTIR spectra of samples B1, B2, B3, and B4.

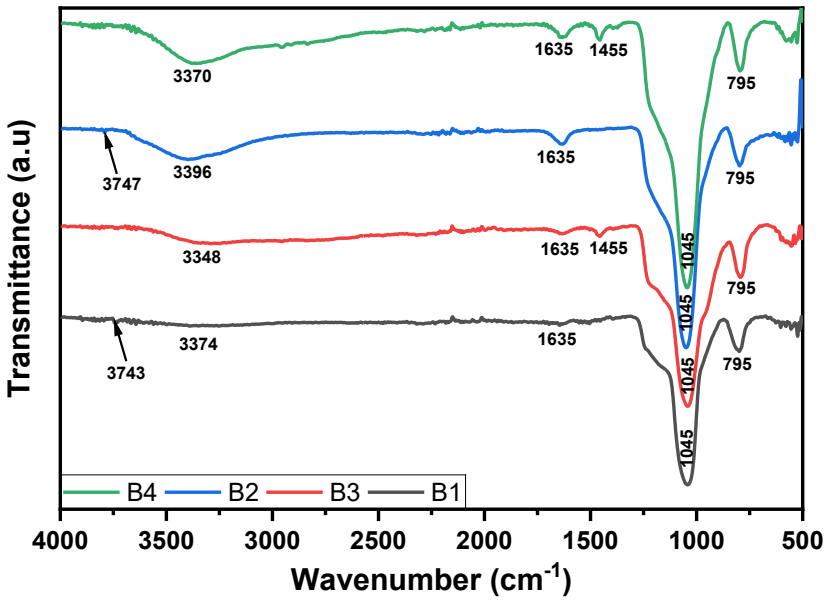

Figure V. 3. FTIR spectra of the four samples B1, B2, B3, and B4.

The FTIR spectra reveal the structural and chemical modifications of the studied materials. Sample B1 exhibits the characteristic bands of MCM-41, notably at 1045 cm^{-1} (asymmetric Si–O–Si vibrations) and 795 cm^{-1} (symmetric Si–O vibrations), as well as a band for free silanols at 3743 cm^{-1} and a broad weak band at 3374 cm^{-1}, attributed to O–H vibrations of physiosorbed water molecules on the silanols [4,8]. The incorporation of aluminum in B2 preserves the silanol band at 3747 cm^{-1} and leads to an intensification of a broad band centered at 3396 cm^{-1} assigned to O–H vibrations of water molecules, indicating an increase in hydrophilicity and, consequently, a change in the polarity of material B2 [9]. A band at 1635 cm^{-1}, weak in B1 but more pronounced in B2, corresponds to bending vibrations of adsorbed water molecules, confirming the increased polarity and affinity of material B2 for water molecules after the introduction of aluminum into the MCM-41 structure [10].

Following MDEA grafting, new bands appear at 1455 cm^{-1}, attributed to bending vibrations of methylene groups (-CH_2-), suggesting covalent bonding with the material surface [11]. The intensification of the 1635 cm^{-1} band in B3 reflects an increase in polarity of the purely siliceous MCM-41 due to MDEA introduction. Furthermore, the disappearance of free silanol bands in B3 and B4, replaced by less intense bands at 3348 cm^{-1} and 3370 cm^{-1} respectively, confirms the substitution of Si–OH groups by organic functions, indicating successful grafting of MDEA on the surfaces of both materials B3 and B4 [12]. The intensification of these bands indicates enhanced hydrophilicity, attributed to the hydroxyl and amine functional groups of MDEA, thereby validating the efficiency of the grafting process [13].

V.1.5. THERMAL ANALYSIS

The thermogravimetric analysis of the studied materials are shown in Figure V.4.

The mesoporous materials investigated reveal distinct but informative thermogravimetric profiles, reflecting both the nature of the porous structure, surface state, and the effect of grafting or aluminum incorporation on thermal behavior. Overall, all samples exhibit two major stages of mass loss, with characteristic temperatures and associated percentages varying subtly according to chemical composition and surface modification.

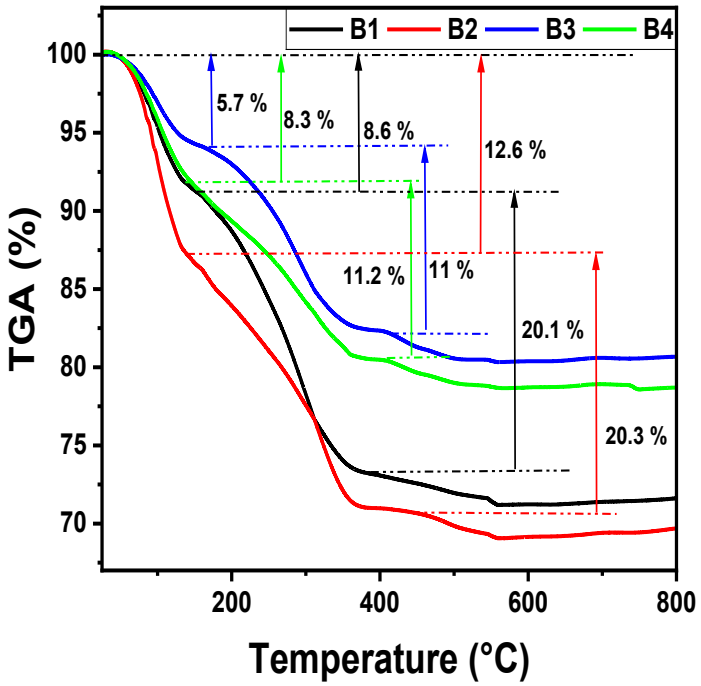

Figure V. 4. Thermogravimetric analysis of the four samples B1, B2, B3, and B4.

The first mass loss, occurring between 94 and 107 °C, is generally attributed to the desorption of physically adsorbed water on the surface or trapped within the pores. This phase is strongly influenced by the surface hydrophilicity, which depends on the presence or absence of hydroxyl sites or metallic elements. Accordingly, sample B2 (Al-MCM-41) exhibits a significant mass loss of 12.6% at 103 °C, reflecting an increased affinity for water molecules as a direct consequence of the presence of aluminum, which introduces Lewis and Brønsted acid sites that promote hydrogen bonding. This interpretation is fully supported by the FTIR results, which revealed, in this same family of materials, characteristic bands around 3396 cm^{-1} and 1635 cm^{-1}, respectively assigned to the stretching and bending vibrations of adsorbed water molecules. In contrast, B3 (MCM-41 grafted with MDEA) shows a more modest loss (5.7% at 98 °C), which could be related to the steric effect induced by the organic grafting that tends to repel ambient moisture. This behavior is further confirmed by the attenuation, and even near disappearance, of the 1635 cm^{-1} band in the FTIR spectra of B3, indicating a lower presence of water associated with the surface. Materials B1 (pure MCM-41) and B4 (grafted Al-MCM-41), with losses of 8.6% and 8.3% respectively between approximately 94–107 °C, occupy an intermediate position, reflecting both the original mesoporous nature and the moderate impact of modification—whether it be the slightly hydrophilic effect due to the presence of silanols in the silicate framework (B1), or the balance between hydrophilicity imparted by aluminum and amphiphilicity (hydrophilic–hydrophobic) resulting from organic grafting (B4).

The second, more pronounced phase of mass loss, observed between 279 and 289 °C, is generally attributed to the thermal decomposition of organic species present in the materials. For the non-grafted samples, notably B1 (MCM-41) and B2 (Al-MCM-41), the significant losses recorded—20.1% at 285 °C and 20.3% at 289 °C, respectively—mainly reflect the thermodegradation of the structuring surfactant (CTABr). The grafted materials, B3 (MCM-41 grafted with MDEA) and B4 (grafted Al-MCM-41), present markedly lower mass losses during this second thermal phase, with 11% at 279 °C for B3 and 11.2% at 283 °C for B4. These losses are attributed to the thermal degradation of the organic groups derived from the MDEA molecule grafted onto the surface. The relatively high temperature of this decomposition clearly indicates that MDEA is covalently grafted rather than merely physically adsorbed on the material surfaces. This distinction confirms the effectiveness of the post-synthesis grafting and also highlights the superior thermal stability of the introduced organic functions, thereby enhancing the robustness of the modified materials under

adsorption conditions. Furthermore, these results clearly demonstrate the structuring and modulating effects of organic grafting as well as aluminum incorporation on the thermal and adsorptive properties of the mesoporous materials.

V.1.6. SCANNING ELECTRON MICROSCOPY

The SEM images of the studied materials are presented in Figure V.5.

The SEM analysis of the four samples reveals significant morphological changes depending on the chemical composition and functionalization. Sample B1, corresponding to pure silica MCM-41, exhibits a well-defined granular morphology with spherical or pseudo-spherical particles uniformly dispersed. The internal structure observed on some fractured particles highlights a characteristic hexagonal arrangement of the mesopores of MCM-41. The surface texture is relatively smooth, indicating good preservation of the porous organization after thermal treatment.

However, sample B2 maintains this overall textural organization but shows some notable differences. The incorporation of aluminum induces a slight roughness on the particles and an increase in aggregation, likely due to enhanced interparticle interactions.

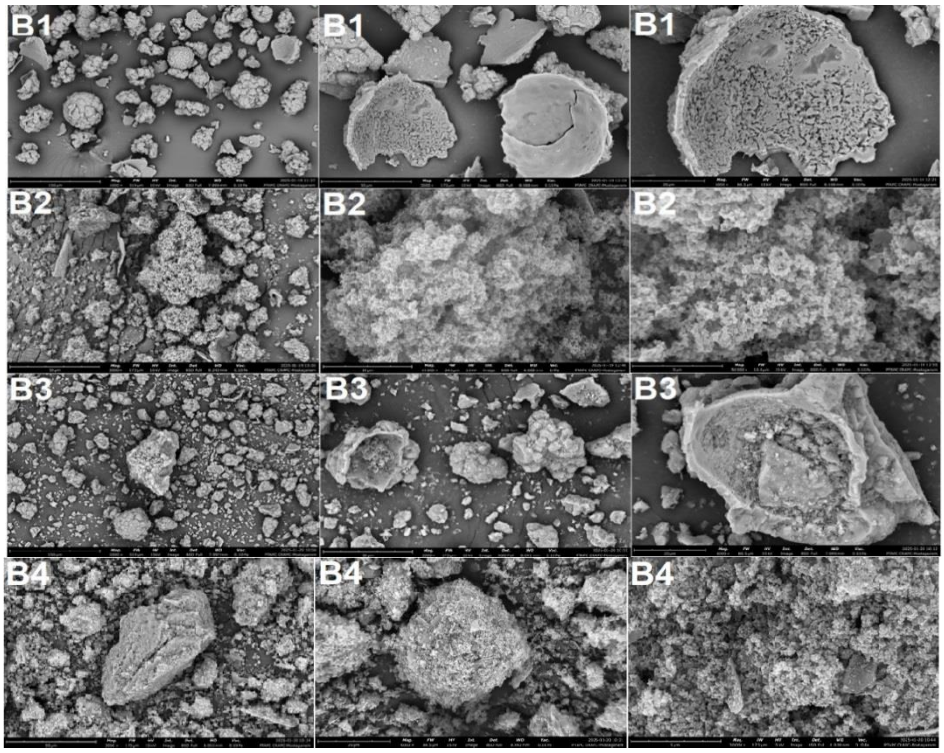

Figure V. 5. SEM images of samples B1, B2, B3, and B4.

The presence of nanoparticle aggregates indicates a modification of interaction forces comparing to purely siliceous MCM-41. At high magnification, the surface texture becomes more heterogeneous, with visible porous zones, suggesting an influence of aluminum on the local structuring of the mesopores.

However, functionalization with MDEA significantly alters the morphology of the materials. Sample B3 shows a strong tendency toward particle aggregation, resulting in partial loss of the initial structure. The low-magnification image highlights a reorganization of the grains, likely due to interactions between the MDEA molecules and the siliceous surface. At higher magnification, textural irregularities appear, suggesting possible partial pore blockage or disruption of the mesoporous alignment.

In contrast, sample B4 undergoes even more pronounced transformations. Particle aggregation becomes more extensive, forming denser and less homogeneous structures than those observed in B3. Some areas exhibit a coated appearance, which can be attributed to the grafted molecule. This difference between B3 and B4 suggests stronger interactions between MDEA and the acid sites introduced by aluminum, influencing the distribution and organization of the particles.

These observations confirm that functionalization with MDEA has modified not only the surface texture but also the morphology and particle arrangement, with more significant effects in the presence of aluminum. Such transformations may impact the adsorptive properties of the materials, particularly their textural accessibility and affinity for target molecules.

V.2. ADSORPTION TEST RESULTS

V.2.1. OPTIMIZATION OF CONTACT TIME AND ADSORBENT QUANTITY

In a pollutant adsorption process, the contact time and the amount of adsorbent are two closely related parameters that directly influence the efficiency of the process [14]. Increasing the adsorbent mass and the interaction time generally promotes better adsorption, up to a point of equilibrium where the saturation of active sites limits any further adsorption.

To evaluate this effect, experiments were conducted by varying the adsorbent mass (50 mg, 100 mg, and 150 mg) in a fixed volume of 20 mL of wastewater containing an initial hydrocarbon concentration of 47 ppm. The tests were carried out in beakers under constant

stirring for 60 minutes at room temperature. After adsorption, the Residual Concentration (RC) of hydrocarbons was measured in order to determine the optimal amount of adsorbent. Figure V.6 shows the residual hydrocarbon concentrations for each material at the different tested masses.

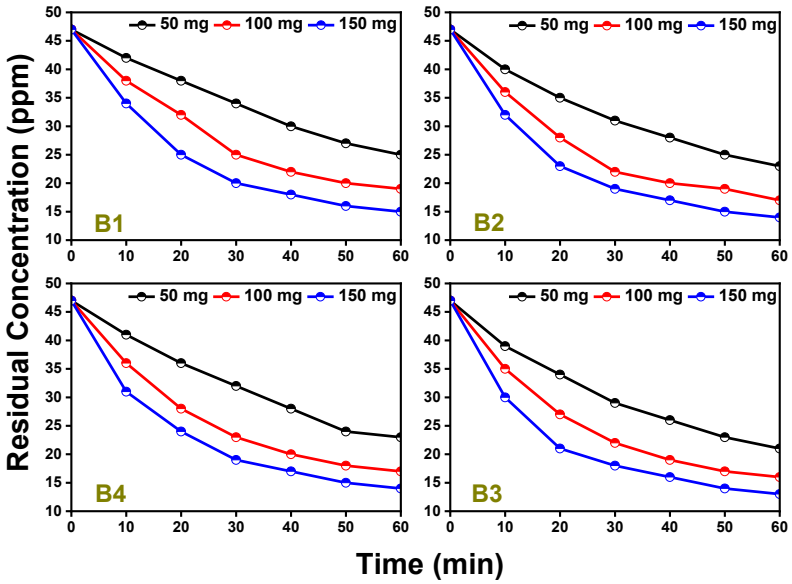

Figure V. 6. Residual hydrocarbon concentrations of materials B1, B2, B3, and B4 at the different tested masses.

The influence of adsorbent mass on hydrocarbon removal highlights a balance between efficiency and material consumption.

At a mass of 50 mg, adsorption remains limited. After 60 minutes, the residual concentration does not drop below 20 ppm, corresponding to a 57.45% reduction from the initial concentration of 47 ppm. This partial adsorption indicates that the amount of adsorbent is insufficient to capture all the hydrocarbons present in solution.

Increasing the mass to 100 mg significantly improves the efficiency. For all materials, the concentration drops below 20 ppm well before the 60-minute mark, reaching retention rates above 57.45% and confirming this quantity as an optimal compromise between performance and material usage. At 150 mg, adsorption becomes faster at the beginning of the process, allowing a more pronounced reduction in hydrocarbons within the first few minutes. However, after 40 to 60 minutes, the difference in efficiency between 100 mg and 150 mg becomes negligible, indicating saturation of the active sites.

The performance of the materials shows marked contrasts depending on their composition and modification. B1, a purely siliceous material, exhibits moderate adsorption, with higher

residual hydrocarbon concentrations compared to B2. The absence of acidic sites limits specific interactions, thereby reducing overall efficiency. In contrast, B2, enriched with aluminum, contains additional acidic sites that enhance interactions with hydrocarbons—especially polar ones—accelerating the decrease in residual concentration and significantly improving adsorption. Post-synthesis chemical modifications further enhance these performances: B3 outperforms its non-grafted counterpart due to altered surface interactions that facilitate hydrocarbon capture. B4 stands out as the best adsorbent, combining the effect of aluminum-acidic sites and specific interactions induced by grafting. This synergy allows minimal residual concentrations to be reached in a reduced time, clearly demonstrating the crucial role of surface modification in optimizing adsorption.

Furthermore, with a stirring duration between 50 and 60 minutes, all materials reach a saturation state where adsorption no longer significantly progresses. However, for the most efficient materials, namely B2 and B4, a duration of 40 minutes appears sufficient to achieve maximum adsorption, indicating a strong affinity between these materials and hydrocarbons. In contrast, for less efficient materials like B1, a prolonged contact time may be necessary to compensate for the lower density of active sites and maximize pollutant capture.

Overall performance analysis leads to the conclusion that using 100 mg of adsorbent offers the best trade-off between efficiency and material consumption. This dosage ensures a significant reduction in hydrocarbon concentration while avoiding unnecessary material excess. Among the studied adsorbents, B4 stands out as the most efficient solution, offering the highest adsorption capacity and the fastest kinetics, making it an excellent candidate for demanding industrial applications. If grafting is not feasible, B2 represents a valuable alternative due to its alumina-based structure, which favors adsorption. B3, although grafted, significantly improves efficiency compared to B1 but does not surpass the performance of alumina-based materials. These results highlight the crucial impact of chemical and structural modifications on optimizing adsorption performance, paving the way for targeted strategies in the treatment of hydrocarbons in industrial effluents.

V.2.2. OPTIMIZATION OF THE ADSORPTION TEMPERATURE

After optimizing the adsorbent dosage to 100 mg and the agitation time to 60 minutes, the effect of temperature on the adsorption efficiency of hydrocarbons by the mesoporous materials was investigated. The temperatures tested were 25°C, 35°C, and 45°C. The Final

Adsorption Capacities (FAC) after 60 minutes for the four materials (100 mg in 20 mL of solution) at different temperatures is presented in Figure V.7.

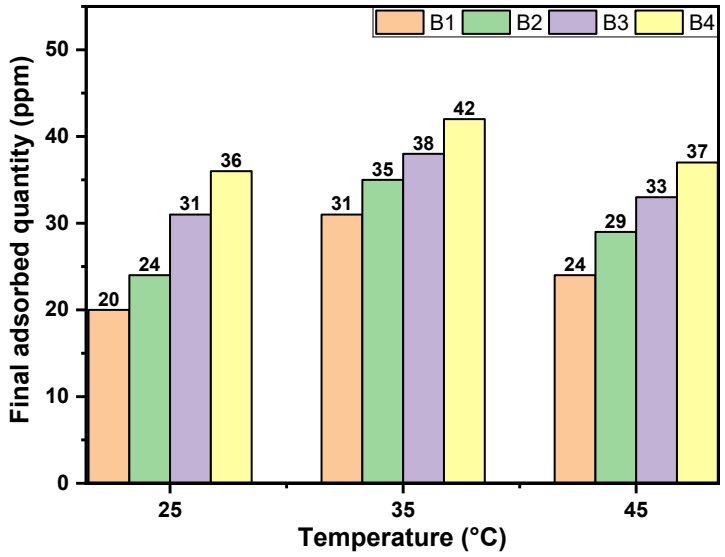

Figure V. 7. Final adsorption capacities of materials B1, B2, B3, and B4 at different temperatures.

The influence of temperature on the adsorption capacity of hydrocarbons was studied at 25 °C, 35 °C, and 45 °C, while maintaining a constant adsorbent mass of 100 mg in 20 mL of solution.

At 25 °C, the adsorption performance follows the same hierarchy previously observed: material B4 exhibits the highest adsorption capacity (36 ppm), followed by B3 (31 ppm), B2 (24 ppm), and finally B1 (20 ppm).

Increasing the temperature to 35 °C significantly improves the adsorption capacity for all materials. This phenomenon can be attributed to enhanced diffusion of hydrocarbons toward the active sites, facilitating their interaction with the adsorbent surface. At this temperature, B4 reaches a maximum capacity of 42 ppm, representing an increase of 16.7% compared to 25 °C. Similarly, B3 increases to 38 ppm (+22.6%), B2 to 35 ppm (+45.8%), and B1 to 31 ppm (+55%). These marked increases demonstrate that temperature promotes diffusion and accessibility of hydrocarbons to the active sites.

However, when the temperature is raised to 45 °C, a slight decrease in adsorption capacity is observed. This decline could be explained by an increase in the kinetic energy of the adsorbed molecules, resulting in partial desorption of hydrocarbons from the adsorbent surface [15]. At this temperature, B4 still retains the highest performance with an adsorption capacity of 37

ppm, although it shows an 11.9% decrease compared to 35 °C. B3 follows with 33 ppm (–13.2%), B2 with 29 ppm (–17.1%), and B1 with 24 ppm (–22.6%).

The analysis of these results highlights that the optimal temperature for adsorption is around 35 °C, where maximum performance is achieved. The efficiency slightly decreases at 45 °C, suggesting that the interaction between hydrocarbons and active sites begins to be affected by desorption phenomena. Among the tested materials, B4 remains the most efficient regardless of temperature, confirming the beneficial effect of the modification introduced to its structure. B3 also shows a notable improvement compared to the unmodified materials, although its performance remains lower than that of B4. Meanwhile, B2 and B1, despite exhibiting lower capacities, follow the same overall trend, underscoring the positive influence of aluminum on adsorption.

These observations confirm that temperature optimization is a key parameter in improving adsorption performance and that a balance between diffusion and hydrocarbon retention is essential to maximize the efficiency of the process.

V.2.3. OPTIMIZATION OF THE MEDIUM'S pH

The influence of the medium’s pH on the maximum adsorption capacity of hydrocarbons was investigated for the four tested mesoporous materials. This analysis is crucial, as pH can simultaneously affect the surface charge of the adsorbent and the state of hydrocarbons in solution, thereby altering the efficiency of the adsorption process [16]. Figure V.8 shows the variation of the final adsorbed capacity as a function of pH, taking into account the three previously studied parameters: adsorbent mass, contact time, and temperature.

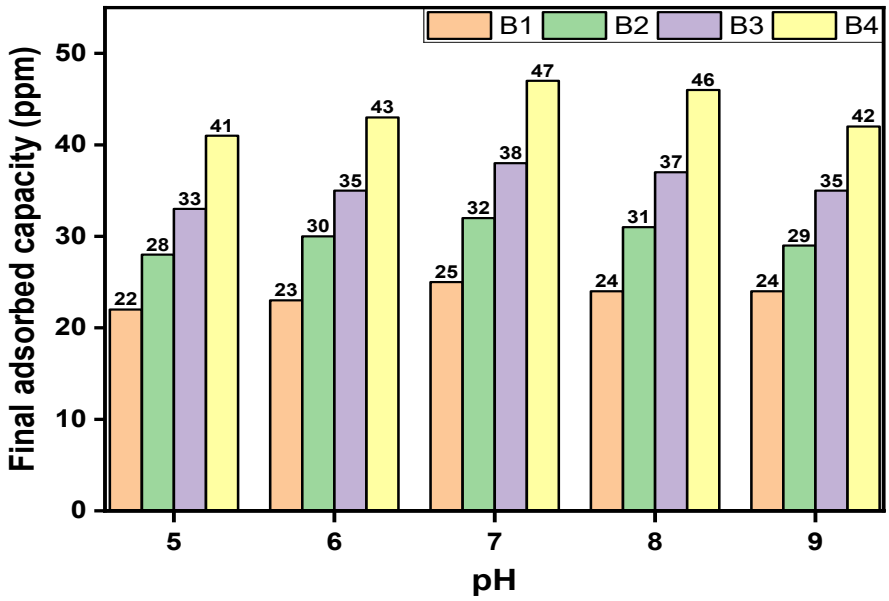

Figure V. 8. Evolution of the final adsorbed capacity of materials B1, B2, B3, and B4 over

The effect of pH on the adsorption capacity of hydrocarbons by the studied mesoporous materials reveals distinct trends directly linked to the interactions between the adsorbent surface and the hydrocarbon molecules in solution.

The influence of pH primarily depends on the surface charge of the materials, the nature of the functional groups present, and the interaction forces involved in the adsorption process [17].

For material B1, the highly siliceous surface has few charged active sites and relies mainly on hydrophobic interactions and Van der Waals dispersion forces [4]. At pH 5, the maximum adsorbed capacity is relatively low, reaching 22 ppm, which can be explained by the increased presence of H^+ ions that may disrupt these interactions and reduce hydrocarbon retention. As the pH increases toward neutral values (pH 7), the surface charge of B1 remains stable, favoring a better affinity between the nonpolar hydrocarbons and the material's surface, thereby reaching a maximum capacity of 25 ppm—an increase of 13.6% compared to pH 5. However, at higher pH (pH 9), the deprotonation of remaining silanol groups may induce repulsive effects, slightly reducing the adsorption capacity to 24 ppm.

The increase in adsorption capacity observed with material B2 is attributed to the presence of aluminum in its structure, which introduces Lewis and Brønsted acid sites playing a key role in adsorbent–adsorbate interactions. At low pH (pH 5), these sites may be heavily protonated, thus reducing their availability for hydrocarbon interaction, resulting in an adsorption capacity of 28 ppm. However, as the pH rises to neutral values, the surface charge becomes more

favorable, enhancing hydrophobic and dipole interactions, leading to a capacity of 32 ppm at pH 7—an improvement of 14.3% compared to pH 5. When the pH becomes more basic (pH 9), desorption effects or competition with solution ions may explain the slight decrease in maximum adsorption capacity to 29 ppm.

The effect of organic grafting on MCM-41 is clearly reflected in the enhanced adsorption capacity of material B3. The introduction of the alcoholamine function (MDEA) modifies the nature of surface interactions by strengthening both hydrophilic and hydrophobic affinities and reducing sensitivity to charge variations. At pH 5, the final adsorption capacity is 33 ppm—a value already higher than that of the non-grafted materials—suggesting better hydrocarbon interaction despite the slightly protonated state of the organic groups. From pH 7 onwards, the surface becomes more stable and the hydrophilic–hydrophobic interactions of the grafted molecule dominate, achieving optimal adsorption at 38 ppm—an increase of 15.2% compared to pH 5. However, at higher pH values (pH of 8 and 9). The maximum adsorption capacity slightly decreases, reaching 37 ppm (a 2.6% drop) and 35 ppm (a 7.9% drop) respectively, relative to the peak value. These values nevertheless remain close to that measured at pH 7. This decrease may be attributed to subtle changes in the interactions between hydrocarbons and the basic functional groups of the grafted material. In fact, under basic conditions, the increased solubility of hydrocarbons in the aqueous phase may reduce their affinity for the active MDEA sites, thereby limiting their adsorption onto the surface.

The best-performing material, B4 (MDEA-Al-MCM-41), combines the synergistic effects of aluminum incorporation and organic grafting with MDEA. Aluminum imparts increased polarity to the material, promoting electrostatic interactions, while organic grafting simultaneously enhances both polar and nonpolar interactions, thereby stabilizing adsorption performance across a wide pH range. At pH 5, its adsorption capacity reaches 41 ppm, already outperforming all other materials tested at this pH. At pH 6, this capacity increases further to 43 ppm, a 4.9% improvement over pH 5. Under neutral conditions (pH 7), an optimal synergy between the specific interactions of MDEA and the coordination forces of aluminum with hydrocarbons allows for a maximum capacity of 47 ppm, corresponding to complete removal of the initial pollutant load—thus reflecting 100% efficiency. Furthermore, unlike the other materials, B4 maintains remarkable efficiency even under mildly basic conditions, with 46 ppm at pH 8 and 42 ppm at pH 9. This behavior indicates a high stability of active sites and low sensitivity to surface charge variations.

It is important to note that, regardless of the pH value, this material demonstrated a high adsorption capacity, maintaining residual total hydrocarbon concentrations in the treated water well below the current Algerian regulatory limit, set at 10 ppm for hydrocarbon discharges in industrial effluents [18].

The variation in maximum adsorption capacities as a function of pH thus highlights the critical role of the physicochemical characteristics of each material in the hydrocarbon adsorption mechanism. The competition between hydrophilic and hydrophobic interactions, Van der Waals forces, protonation/deprotonation effects, and coordination with metal or organic sites explains the observed trends. Under neutral conditions (pH = 7), optimal conditions are achieved for maximizing adsorption, particularly for modified materials, which offer more specific interactions and better adaptability to the constraints of the adsorption environment.

CONCLUSION OF THE ADSORPTION SECTION

The study of hydrocarbon adsorption on mesoporous materials MCM-41, Al-MCM-41, and their MDEA-grafted counterparts allowed the identification of optimal conditions to maximize their performance. The analysis of key parameters (adsorbent amount, agitation time, temperature, and pH) revealed significant trends that guide the optimization of the adsorption process. Optimization of the adsorbent quantity showed that 100 mg represents an ideal compromise, ensuring high adsorption efficiency without premature saturation of active sites. Further increasing the adsorbent amount did not provide significant gains in specific adsorption, indicating a limitation in the available surface capacity. However, agitation time proved crucial in reaching adsorption equilibrium. Duration of 60 minutes was identified as optimal, guaranteeing saturation of active sites without causing desorption effects or unfavorable system rebalancing.

Regarding the temperature effect, adsorption improved when increasing from 25 °C to 35 °C, where the enhanced thermal energy promoted interactions between hydrocarbons and the mesoporous surfaces without compromising adsorbent stability. However, raising the temperature to 45 °C resulted in a slight decrease in adsorption capacity, likely due to desorption induced by excess thermal energy of hydrocarbon molecules. Furthermore, pH showed a decisive influence, especially for the grafted materials. Maximum adsorption was observed in the pH range of 7 to 8, where the stability of active sites and the synergy between

hydrophobic and dipolar interactions were optimal. At pH 5, a notable decrease in performance was recorded, particularly for MDEA-grafted materials, due to protonation of basic sites (hydroxides and the MDEA amine), limiting their ability to interact with hydrocarbons. At pH 9, a slight efficiency drop was observed, attributed to competition with hydroxide ions (for Lewis and Brønsted sites) in solution and increased desorption effects.

From a structural perspective, the incorporation of aluminum into the mesoporous network of MCM-41 (forming Al-MCM-41) significantly enhanced adsorption capacity due to the presence of additional Lewis and Brønsted acid sites, favoring interactions with hydrocarbons of both polar and nonpolar nature. The most pronounced effect was observed with Al-MCM-41 grafted with MDEA, which combined the advantages of aluminum centers and the organic alkanolamine functions of MDEA, thus providing the best adsorption performance across the studied pH range. These results highlight the importance of adsorbent material design and operational condition optimization to improve hydrocarbon removal from industrial effluents. Organic grafting and structural modification via aluminum incorporation appear as promising strategies for developing efficient and robust adsorbents suitable for various environmental conditions.

Moreover, previous studies on hydrocarbon adsorption from industrial wastewater using mesoporous materials, notably MCM-41 and its functionalized derivatives, have highlighted diverse and complementary approaches that inform our investigation. Maretto et al. explored the use of alumina-containing mesoporous silica (MSA) for benzene and toluene removal, emphasizing the influence of Lewis acid interactions on adsorption and the impact of water on pollutant desorption [19]. Similarly, Albayati and Kalash studied naphthalene adsorption by comparing three types of MCM-41, demonstrating that non-calcined and functionalized materials exhibited superior adsorption performance in batch mode, while the calcined form was more suitable for continuous fixed-bed systems. Their study also revealed that adsorption followed pseudo-second-order kinetic models and that the process was exothermic [20]. Additionally, Costa et al. developed an MCM-41-NH2 material from rice husk ash for the adsorption of several polycyclic aromatic hydrocarbons (PAHs), showing high efficiency with removal rates above 80%, notable thermal stability, and optimal affinity at pH 5.6. These works converge on the importance of mesoporous structure and surface chemistry of MCM-41 in optimizing hydrocarbon retention [21]. Building on these advances, our study proposes an innovative approach exploiting the functionalization and adaptation of these materials to specific industrial conditions, thus offering a better understanding of adsorbent-pollutant

interactions and an increased potential for practical applications in treating hydrocarbon-contaminated industrial wastewater.

V.3. MODELING OF ADSORPTION ISOTHERMS

The study of adsorption relies on understanding the physicochemical interactions between the adsorbent and the adsorbate, as well as quantifying the surface retention capacities. After optimizing the experimental conditions, it is essential to evaluate the behavior of the mesoporous materials through modeling of adsorption isotherms. This step allows for the interpretation of the underlying mechanisms and the characterization of the nature of adsorption, whether it is monomolecular (Langmuir type), multimolecular (Freundlich type), or influenced by specific interactions (Temkin model).

Based on experiments conducted under optimized conditions (100 mg of adsorbent, 20 mL of solution with a pollutant concentration of 47 ppm, agitation for 60 minutes at 35 °C and pH 7), we studied the performance of the four materials. Table V.4 below presents the adsorbed amounts (q_ads, in mg/g) as a function of time for each tested adsorbent (from B1 to B4). These experimental data will then be compared to theoretical adsorption models to identify the most suitable model for each system.

Table V.4. Amounts adsorbed by materials B1, B2, B3, and B4 under optimized experimental conditions.

Time (min)	**q_{ads} B1 (mg/g)**	**q_{ads} B2 (mg/g)**	**q_{ads} B3 (mg/g)**	**q_{ads} B4 (mg/g)**
0	0	0	0	0
10	1,6	1,4	2	2,8
20	2,8	3	3,6	5,2
30	3,6	4,2	5,2	7,2
40	4,2	5	6,4	8,6
50	4,6	5,8	7,2	9,2
60	5	6,4	7,6	9,4

The kinetic data analysis reveals clear differences among the tested materials, highlighting the impact of chemical functionalization on adsorption efficiency. Material B1, corresponding to pure MCM-41, exhibits moderate adsorption, reaching a capacity of 5 mg/g after 60 minutes. The introduction of aluminum into the mesoporous framework (B2) improves performance,

with capacity increased to 6.4 mg/g, reflecting the role of polar centers in interactions with hydrocarbons. The grafting of the organic molecule MDEA onto MCM-41 (B3) results in an even more pronounced improvement, reaching 7.6 mg/g, due to additional polar and non-polar interactions induced by the functional groups of MDEA. Finally, the synergistic combination of aluminum incorporation and organic grafting in material B4 achieves a maximum capacity of 9.4 mg/g, confirming that dual modification—both mineral and organic—provides optimal affinity toward hydrocarbons. These results thus emphasize the strategic interest of controlled functionalization of mesoporous materials for effective treatment of wastewater loaded with hydrophobic compounds.

However, to model the adsorption isotherms of methanol on the studied mesoporous materials, the experimental adsorption data were analyzed using the Langmuir, Freundlich, and Temkin models.

Langmuir's model is based on monolayer adsorption. Its isotherm is represented by the following equation (Eq. III.1):

$$q_e = \frac{q_m K_L C_e}{1 + K_L C_e} \qquad \text{(Eq. V.1)}$$

Where:

q_e: the amount of adsorbate adsorbed at equilibrium (mg/g);

q_m: the maximum monolayer adsorption capacity (mg/g);

C_e : the equilibrium concentration of the adsorbate in solution (mg/L);

K_L: the Langmuir constant, representing the affinity of the adsorbent for the adsorbate.

The linearized form of the Langmuir isotherm equation is expressed as follows:

$$\frac{1}{q_e} = \frac{1}{q_m K_L C_e} + \frac{1}{q_m} \qquad \text{(Eq. V.2)}$$

The Freundlich model, which accounts for the heterogeneity of the adsorbent surface, is represented by the empirical equation (Eq. V.3):

$$q_e = K_F C_e^{\frac{1}{n}} \qquad \text{(Eq. V.3)}$$

Where:

The linearization of the Freundlich isotherm equation is expressed as follows:

$$\ln q_e = \ln(K_F) + \frac{1}{n_F} \ln(C_e) \qquad \text{(Eq. V.4)}$$

K_F : the Freundlich constant, representing the adsorption capacity;

$\frac{1}{n_F}$: a parameter indicating the intensity of adsorption.

In the Temkin model, adsorption is described by considering that the adsorption energy decreases linearly with increasing surface coverage due to adsorbate–adsorbate interactions.

$$q_e = B \ln(A_T . C_e) \qquad \text{(Eq. V.5)}$$

Where:

q_e: Amount adsorbed at equilibrium (mg/g).

C_e: Equilibrium concentration of the adsorbate (mg/L).

A_T: Temkin isotherm equilibrium binding constant (L/mg).

$B = \frac{RT}{b}$: Constant related to the heat of adsorption, where R is the universal gas constant (8.314 J/mol·K), T is the temperature (K), and b is the Temkin isotherm constant linked to the adsorption energy.

The linearized form of the Temkin isotherm equation is expressed as follows:

$$q_e = B \ln A_T + B \ln C_e \qquad \text{(Eq. V.3)}$$

The experimental isotherm parameters of the three models (Langmuir, Freundlich, and Temkin), represented by equations V.1, V.2, and V.3, are summarized in Table V.5.

Table V.5. Experimental parameters of the isotherms for the three models used for the different adsorbents.

Matériau	Langmuir			Freundlich			Temkin		
	q_m (mg/g)	K_L (L/mg)	R^2	n_F	K_F (mg/g)	R^2	A_T (L/g)	B (J/mol)	R^2
B1	20,38	1,200	0,792	2,055	8680,66	0,942	1,44 x 10^{11}	0,151	0,988
B2	16,37	1,064	0,612	1,652	10002,3	0,880	5,02 x 10^{9}	0,175	0,975
B3	9,53	0,582	0,597	0,990	30 437,2	0,877	1,3 x 10^{8}	0,214	0,953
B4	1,50	0,318	0,277	0,412	2 810 848,2	0,711	1,65 x 10^{5}	0,363	0,800

Comparative analysis of the Langmuir, Freundlich, and Temkin isotherm models applied to the adsorption of hydrocarbons by mesoporous materials MCM-41, Al-MCM-41, and their MDEA-grafted derivatives reveals distinct behaviors reflecting the diversity of interaction mechanisms between the adsorbents and the organic phase in solution.

The Langmuir model, based on the assumption of monolayer adsorption on a homogeneous surface, fits moderately well for the non-grafted materials, with correlation coefficients (R^2)

of 0.792 for B1 and 0.612 for B2, but shows poor relevance for the grafted materials B3 and B4—particularly B4, where R^2 drops to 0.277—suggesting pronounced surface heterogeneity and multiple interactions incompatible with the model. The theoretical maximum adsorption capacities q_m decrease from B1 (20.38 mg/g) to B4 (1.5 mg/g), in contradiction with the actual adsorbed amounts, further confirming the inadequacy of the Langmuir model in describing adsorption onto modified materials. The Freundlich model, which accounts for adsorption on a heterogeneous surface, provides a better fit, especially for B1 (R^2 = 0.942) and B2 (R^2 = 0.880), with significant K_F constants (8680 and 10002 mg/g, respectively), indicating good affinity of the materials for hydrocarbons. However, for B3 and B4, although K_F reaches very high values (up to 2.8×10^6 mg/g for B4), the low values of nF (below 1) and $R^2 < 0.9$ suggest less favorable adsorption, possibly hindered by steric effects related to grafting or diffusion limitations. In contrast, the Temkin model proves to be the most suitable for describing adsorption on these materials, with very high correlation coefficients (R^2 = 0.988 for B1, 0.975 for B2, and 0.953 for B3), indicating adsorption governed by adsorbent–adsorbate interactions with variable energy. The parameter B, representing the distribution of adsorption energy, increases progressively from B1 (0.151 J/mol) to B4 (0.363 J/mol), reflecting a gradual intensification of the adsorbent–adsorbate interactions. This trend highlights the structuring and beneficial effect of aluminum incorporation combined with MDEA grafting, which imparts a more reactive surface better suited to interact with hydrocarbons. This enhancement in energetic interactions underscores the effectiveness of organic grafting as a strategy to improve the performance of mesoporous adsorbents, thereby confirming the added value of the process developed in this work. The extremely high AT value for B1 (1.44×10^{11} L/g) and its decreasing magnitude for B2, B3, and B4 further confirm the significant modifications of the adsorbent surface due to the introduction of aluminum and MDEA. Thus, although the grafted materials exhibited the best practical performance in terms of adsorption capacity, their complex behavior appears to be more accurately described by the Temkin model, underscoring the importance of a multi-model approach to precisely characterize adsorption phenomena in functionalized systems with heterogeneous surfaces.

Bibliographic references

[1] Z. Rahimi, A.A. Zinatizadeh, S. Zinadini, M. van Loosdrecht, H. Younesi, A new anti-fouling polysulphone nanofiltration membrane blended by amine-functionalized MCM-41 for post treating waste stabilization pond's effluent, Journal of Environmental Management 290 (2021) 112649.

[2] B. Boukoussa, S. Zeghada, G.B. Ababsa, R. Hamacha, A. Derdour, A. Bengueddach, F. Mongin, Catalytic behavior of surfactant-containing-MCM-41 mesoporous materials for cycloaddition of 4-nitrophenyl azide, Applied Catalysis A: General 489 (2015) 131–139.

[3] J.O.Tella, K.O. Ajanaku, J.A. Adekoya, R. Banerjee, C.R. Patra, S. Pavuluri, B. Sreedhar, Physicochemical and textural properties of amino-functionalised mesoporous silica nanomaterials from different silica sources, Results in Chemistry 7 (2024) 101505.

[4] B. Boukoussa, R. Hamacha, A. Morsli, A. Bengueddach, Adsorption of yellow dye on calcined or uncalcined Al-MCM-41 mesoporous materials, Arabian Journal of Chemistry 10 (2017) S2160–S2169.

[5] N. Chouat, A. Maziz, B. Bensafi, F. Djafri, Hierarchized ZSM-5 Zeolite Synthesis using *N*-Methyldiethanolamine as a Novel Desilicate Agent: Impact on Methanol Adsorption and Resistance Improvement to Coke Poisoning, Journal of Inorganic and Organometallic Polymers and Materials 34 (2024) 5154–5164.

[6] M. Thommes, K. Kaneko, A.V. Neimark, J.P. Olivier, F. Rodriguez-Reinoso, J. Rouquerol, K.S.W. Sing, Physisorption of gases, with special reference to the evaluation of surface area and pore size

distribution (IUPAC Technical Report), Pure and Applied Chemistry 87 (2015) 1051–1069.

[7] S. Loganathan, A.K. Ghoshal, Amine tethered pore-expanded MCM-41: A promising adsorbent for CO_2 capture, Chemical Engineering Journal 308 (2017) 827–839.

[8] P. Iliade, I. Miletto, S. Coluccia, G. Berlier, Functionalization of mesoporous MCM-41 with aminopropyl groups by co-condensation and grafting: a physico-chemical characterization, Research on Chemical Intermediates 38 (2012) 785–794.

[9] A. Jentys, N.H. Pham, H. Vinek, Nature of hydroxy groups in MCM-41, Journal of the Chemical Society, Faraday Transactions 92 (1996) 3287–3291.

[10] I.C.B. Pires, S.I. Shuchi, B.V.A. Tostes, D.K.D.N. Santos, W.L. Burnett, B.C. Leonce, O.R. Harvey, J.L. Coffer, I.A.S. Filho, P.F de Athayde-Filho, S.A. Junior, J.M. Mathis, Theranostics Using MCM-41-Based Mesoporous Silica Nanoparticles: Integrating Magnetic Resonance Imaging and Novel Chemotherapy for Breast Cancer Treatment, International Journal of Molecular Sciences 25 (2024) 8097.

[11] P. Iliade, I. Miletto, S. Coluccia, G. Berlier, Functionalization of mesoporous MCM-41 with aminopropyl groups by co-condensation and grafting: a physico-chemical characterization, Research on Chemical Intermediates 38 (2012) 785–794.

[12] D. Mudhakir, E. Sadaqa, Z. Permana, J.E. Mumtazah, N.F. Zefrina, J.N. Xeliem, L.F. Hanum, N.F. Kurniati, Dual-Functionalized Mesoporous Silica Nanoparticles for Celecoxib Delivery: Amine Grafting and Imidazolyl PEI Gatekeepers for Enhanced Loading and Controlled Release with Reduced Toxicity, Molecules 29 (2024) 3546.

[13] S. Mukherjee, Akshay, A.N. Samanta, Amine-impregnated MCM-41 in post-combustion CO_2 capture: Synthesis, characterization, isotherm modelling, Advanced Powder Technology 30 (2019) 3231–3240.

[14] O.P. Murphy, M. Vashishtha, P. Palanisamy, K.V. Kumar, A Review on the Adsorption Isotherms and Design Calculations for the Optimization of Adsorbent Mass and Contact Time, ACS Omega 8(20) (2023) 17407–17430.

[15] B.M. Aumeier, A. Augustin, M. Thönes, J. Sablotny, T. Wintgens, M. Wessling, Linking the effect of temperature on adsorption from aqueous solution with solute dissociation, Journal of Hazardous Materials 429 (2022) 128291.

[16] M. Kosmulski, The pH dependent surface charging and points of zero charge. X. Update, Advances in Colloid and Interface Science 319 (2023) 102973.

[17] B. Wang, X. Gao, R. Qiu, Y. Chen, Y. Gao, G. Hu, D. Yu, Adsorption of PFCs and antibiotics from water using mesoporous silica and amino-functionalized mesoporous silicon materials: A review, Chemical Engineering Journal 505 (2025) 159642.

[18] Décret exécutif n° 06-141 du 20 Rabie El Aouel 1427 correspondant au 19 avril 2006 définissant les valeurs limites des rejets d'effluents liquides industriels.

[19] M. Maretto, R. Vignola, C.D. Williams, R. Bagatin, A. Latini, M.P. Papini, Adsorption of hydrocarbons from industrial wastewater onto a silica mesoporous material: Structural and thermal study, Microporous and Mesoporous Materials 203 (2015) 139–150.

[20] T.M. Albayati, K.R. Kalash, Polycyclic aromatic hydrocarbons adsorption from wastewater using different types of prepared mesoporous materials MCM-41in batch and fixed bed column, Process Safety and Environmental Protection 133 (2020) 124–4136.

[21] J.A.S. Costa, V.H.V. Sarmento, L.P.C. Romão, C.M. Paranhos, Performance of the MCM-41-NH_2 Functionalized Mesoporous Material Synthetized from the Rice Husk Ash on the Removal of the Polycyclic Aromatic Hydrocarbons, Silicon 12 (2020) 1913–1923.

General Conclusion

GENERAL CONCLUSION

This thesis work was dedicated to the study of hydrocarbon adsorption from industrial wastewater, highlighting the environmental and scientific significance of this approach as a sustainable solution for the decontamination of polluted aqueous effluents. Through a rigorous methodology based on the synthesis, characterization, and evaluation of mesoporous MCM-41 type materials, grafted or functionalized, we demonstrated the efficiency of adsorption as a high-performance technique suitable for real industrial environments.

Four materials were designed and studied: purely siliceous MCM-41, aluminum-impregnated Al-MCM-41, as well as their derivatives grafted with methyl diethanolamine (MDEA), an amphiphilic organic molecule chosen to enhance surface affinities toward both polar and non-polar hydrocarbons. These materials were prepared using a controlled sol-gel protocol and calcined at high temperature, then characterized by several complementary techniques. X-ray diffraction (XRD) analysis confirmed the preservation of the ordered hexagonal structure for the parent materials, whereas the grafted derivatives exhibited slight peak shifts, suggesting a controlled disruption of the crystalline organization. X-ray fluorescence (XRF) analysis allowed monitoring of aluminum incorporation, with a Si/Al ratio near 45, and revealed the effect of grafting on chemical composition, notably a slight dealumination linked to MDEA introduction. BET analysis highlighted a high specific surface area for the parent materials (up to 1411 m^2/g), with a marked decrease after grafting, reflecting the partial filling of mesopores by functional groups. FTIR spectroscopy confirmed the appearance of characteristic bands of the amine groups of MDEA, while thermogravimetric analysis (TGA) revealed two major mass loss steps: the first related to desorption of surface water and the second to thermal decomposition of the grafted organic molecules or structuring agents. FTIR results, correlated with TGA, further confirmed the presence of surface water on hydrophilic materials, especially on aluminum-doped samples. Scanning electron microscopy (SEM) visualized morphological changes induced by grafting, with a more irregular surface and better-exposed porosities.

On the application side, the materials were tested for hydrocarbon adsorption from real industrial wastewater samples collected from a CPI treatment unit, optimizing experimental parameters such as adsorbent mass, agitation time, temperature, and pH. The most remarkable performances were obtained with the grafted Al-MCM-41 material, exhibiting an adsorption

capacity of 9.4 mg/g and 100% pollutant removal efficiency after 60 minutes at pH of 7 and temperature of 35 °C, reflecting the synergistic effect between acidic sites introduced by aluminum and grafted organic groups. The pH influence study showed that all materials reached maximum adsorption near neutrality, and that B4 maintained a capacity above 42 ppm even in media far from neutrality, demonstrating its operational robustness. Adsorption isotherm modeling showed good fitting of experimental data to the Freundlich model, suggesting multilayer adsorption on a heterogeneous surface. The Temkin model also yielded consistent results, particularly regarding progressive adsorption influenced by the energetic distribution of adsorption sites. Compared to similar studies in the literature, the grafted materials developed here demonstrate comparable or even superior performance to amine-functionalized adsorbents, while maintaining promising thermal stability and regenerability. The originality of this work lies in the dual modification of mesoporous surfaces combining metal doping and organic functionalization, as well as the in-depth study of correlations between structure, textural properties, and adsorption capacities under real conditions.

This integrated approach offers an effective pathway for developing tailor-made materials aimed at advanced wastewater treatment. In summary, this thesis demonstrated the relevance of mesostructured material engineering for targeted adsorption of organic pollutants. It opens promising perspectives, including extension to other contaminant classes, study of dynamic column behavior, and optimization of adsorption–desorption cycles for regeneration and reuse. In the long term, integrating these materials into industrial treatment units could provide a sustainable, innovative, and adaptable solution to current environmental requirements.